Spring 2017

Design and Performance Analysis of Small Scale Horizontal Axis Wind Turbine for Nano Grid Application

Md Mehedi Hasan

DESIGN AND PERFORMANCE ANALYSIS OF SMALL SCALE HORIZONTAL AXIS WIND TURBINE FOR NANO GRID APPLICATION

by

MD MEHEDI HASAN

(Under the Direction of Adel El Shahat)

ABSTRACT

Wind energy, being easily accessible, environmentally friendly, and cost effective, has become one of the world's popular growing renewable energy sources of electricity generation. To spread this technology to mankind it is necessary to develop turbines in this way that people can use it individually and comfortably. This kind of thinking accelerates the advancement of integration of wind turbine with Nano grid concept. Although significant progress has been achieved in the wind technology, there is still scope to reduce the cost and improve the performance of small-scale wind turbines. Moreover, low wind velocity also needs to be utilized properly to achieve saturated energy production. So, concentration is going to small scale wind. Small scale wind energy systems such as Small Scale Horizontal Axis Wind Turbines (SSHAWT), and Vortex Blade-Less (VBL) wind generators can provide a clean, prospective and viable option for energy supply. Moreover, this energy consumption system can also be utilized as one of the reliable power sources of Nano grid. To design efficient wind technologies a smooth and continuous development process is required. The first part of the current study focused on the aerodynamic design and performance analysis of small-scale horizontal axis wind turbine blade using the blade element momentum (BEM) method with the most updated and corrected model.

In this case, the blade was designed with a single airfoil. Results show that the maximum coefficient of performance is 0.446 at the tip speed ratio 6.5 which is very good indication in preliminary stage power prediction. The 2nd part of the study concentrated on improving blade performance by modifying the blade with a combination of three airfoils. After that, a comparative study was done between "Blade-Element-Momentum" (BEM) analysis and "Computational-Fluid-Dynamics" (CFD) analysis of mixed airfoil small-scale horizontal axis wind turbine blades. In CFD analysis, k-ω "Shear-Stress-Transport" (SST) model was conducted for three-dimensional visualization of turbine performance. The pitch is considered as fixed and rotor speed is variable for both of the studies. However, the best coefficient of performance was observed at 6° angle of attack. At this angle of attack, in the case of BEM, the highest coefficient of performance is 0.47 whereby CFD analysis, is 0.43. Both studies show good performance prediction which is a positive step to accelerate the continuous revolution in the wind energy sector. However, as an extension of continuous study on small-scale wind energy systems, the aim of the 3rd part is to investigate the possible extraction of power from wind energy by using new conceptual vortex bladeless wind generators. In this work, design parameters were selected based on the Von Karman effect. After that, a mathematical model was developed to get maximum lift force generated by the designed body. Finally, a complete model was recommended by fluid-structure interaction (FSI) simulation to get a clear idea of extracted vibration energy from vortex bladeless wind generator for further conversion to electricity generation.

INDEX WORDS: Renewable energy, Wind energy, Wind turbine, Small scale, BEM, CFD, Vortex Bladeless, Von-Karman, FSI.

DESIGN AND PERFORMANCE ANALYSIS OF SMALL-SCALE HORIZONTAL AXIS WIND TURBINE FOR NANO GRID APPLICATION

by

MD MEHEDI HASAN

B. S., Khulna University of Engineering and Technology, Bangladesh, 2013

A Thesis Submitted to the Graduate Faculty of Georgia Southern University in Partial Fulfillment of the Requirements for the Degree

MASTER OF SCIENCE

STATESBORO, GEORGIA

DESIGN AND PERFORMANCE ANALYSIS OF SMALL-SCALE HORIZONTAL AXIS WIND TURBINE FOR NANO GRID APPLICATION

by

MD MEHEDI HASAN

Major Professor: Adel El Shahat

Committee: Mohammad Ahad

Rami Haddad

Electronic Version Approved:
May 2017

DEDICATION

This thesis work is dedicated to my beloved parents, for their unwavering support and inspiration throughout my education life. Also, I would like to dedicate this work to my sister, for her constant support and encouragement.

ACKNOWLEDGEMENTS

First of all, I express my profound gratitude to my thesis supervisor, Dr. Adel El Shahat, Department of Electrical Engineering, Georgia Southern University for enlightening me about the utmost importance of small-scale wind energy. It was a pleasure to work with him and learn the different factors of research. I wish to express my heartiest thanks and a deep sense of gratitude to him for his deep insights, unequivocal and continuous guidance, valuable suggestions and encouragement in every stage of my progress.

I also thank my parents and all family members and friends for their encouragement and love during my thesis work.

Lastly, I express my gratitude to authors of all reference papers, books, and websites as mentioned in references section which is necessary for the research.

Table of Contents

LIST OF FIGURES

LIST OF TABLES

LIST OF SYMBOLS

Symbol	Explanation
R_e	Reynold Number
V	Air Speed (m/s)
μ	Dynamic Viscosity (N.s/m²)
v	Kinematic Viscosity (m²/s)
ρ	Air Density (kg/m^3)
q_{ref}	Reference Pressure (Pa)
D	Drag Force (N)
C_D	Drag Coefficient
L	Lift Force (N)
C_L	Lift Coefficient
F_T	Tip Loss Correction Factor
F_R	Root Loss Correction Factor
F_S	Side Force (N)
$\dot{m}$	Mass Flow Rate (kg/s)
P	Pressure (Pa)
P_T	Total Pressure (Pa)
P_S	Static Pressure (Pa)
T	Thrust (N)
A	Cross Sectional Area (m²)
a	Axial Induction Factor
a'	Tangential Induction Factor

C_P	Coefficient of Power
C_T	Coefficient of Thrust
Q	Torque (Nm)
γ	Tip Speed Ratio
U_T	Tangential Velocity (m/s)
U_A	Axial Velocity (m/s)
W	Relative Wind Velocity (m/s)
α	Angle of Attack (0°)
σ	Blade Solidity
θ	Yaw Angle (0°)
$\emptyset$	Angle of Relative Wind Velocity (0°)
β	Local pitch angle (0°)

CHAPTER 1

INTRODUCTION

1.1 Background

The utilization of energy resources has played a key role in the development of human civilization. Now one of the greatest challenges in a modern century is to find out the reliable energy source. Conventional energy sources such as natural gas, coal, and fossil fuel have accelerated industrialization and modernization of different nations. However, the consternation around the world is that the emission of carbon dioxide into the atmosphere produced due to these traditional sources is the number one offender for the climate change. Climate change has the massive impact on the environment such as increased pollution, flooding, drought, the rise in sea levels, high temperature, etc. Moreover, the rise in ocean temperature and the acidity levels cause major changes to the natural ecosystems. So today's burning question is that, besides producing sufficient energy for mankind could we be able to ensure a safe world for next generation? Hence, it should be committed to finding out the solution of using alternative energy resources besides the conventional sources. For this reason, renewable and sustainable energy is getting attention in current research.

However, one of the greatest difficulties in this century is to produce adequate energy. The expansion in world population and the persistent economic growth in many countries require more access to energy. Renewable and sustainable energy is gradually gaining interest in recent research due to the considerations on the depleting nature of non-renewable resources and availability of renewable energy resources. It is necessary for any nation to pursue solutions or alternatives in

renewable energy resources with current technologies and low cost in maintenance and operation. Renewable energy (for example solar, wind, and biofuel, hydro) have shown to be a feasible alternative sources of energy to other renewable sources of energy. Nowadays, renewable energy is one of the key sources of electric power generation. According to Global Energy Statistical Yearbook 2016, Figure 2 has statistics of electricity production from renewable energy in different countries of the world.

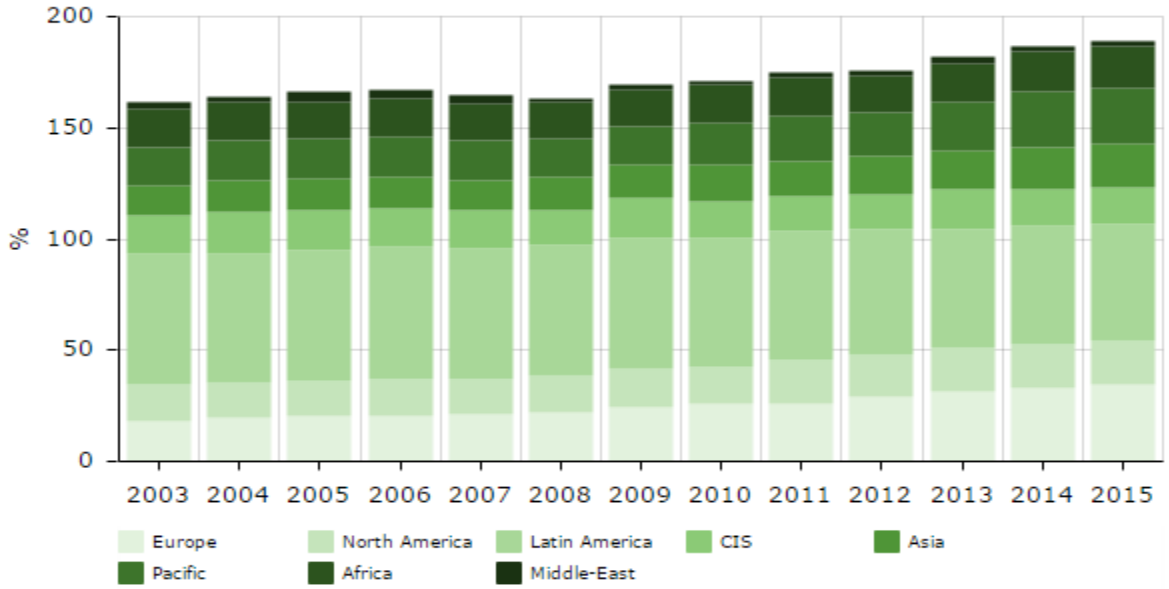

Figure 1: Electricity production by renewable energy in major world portion (Enerdata, 2016) .

It is noticeable that about 13.44 percent of total U.S. domestic electricity generation comes from renewable energy sources (Enerdata, 2016). Among all the renewable energy sources, wind energy, being easily accessible, environmentally friendly, and being cost effective, has become one of the world's popular growing renewable energy sources of electricity generation. Wind power is considered as the most significant and never ending potential resource. However, wind turbine technology can be utilized as a prime mover operated by such type of renewable energy source.

In spite of the fact that the wind energy industry is moderately new, it has become one of the quickest-developinging energy sources in the world. This is mainly due to the spread of the technology and low operating cost compared to other sustainable power sources. Commercial wind turbines have expanded significantly in size, which has ensued in more energy being extracted from the wind. According to the Global Wind Energy Council (GWEC), the total installed global wind power capacity is nearly 487 GW. The leading countries in the wind energy sector are the US, China, Germany, and India. Moreover, also unexpectedly strong showings from France, Turkey and the Netherlands (GWEC, 2017). The global cumulative installed wind capacity 2001-2016 is shown in figure 2.

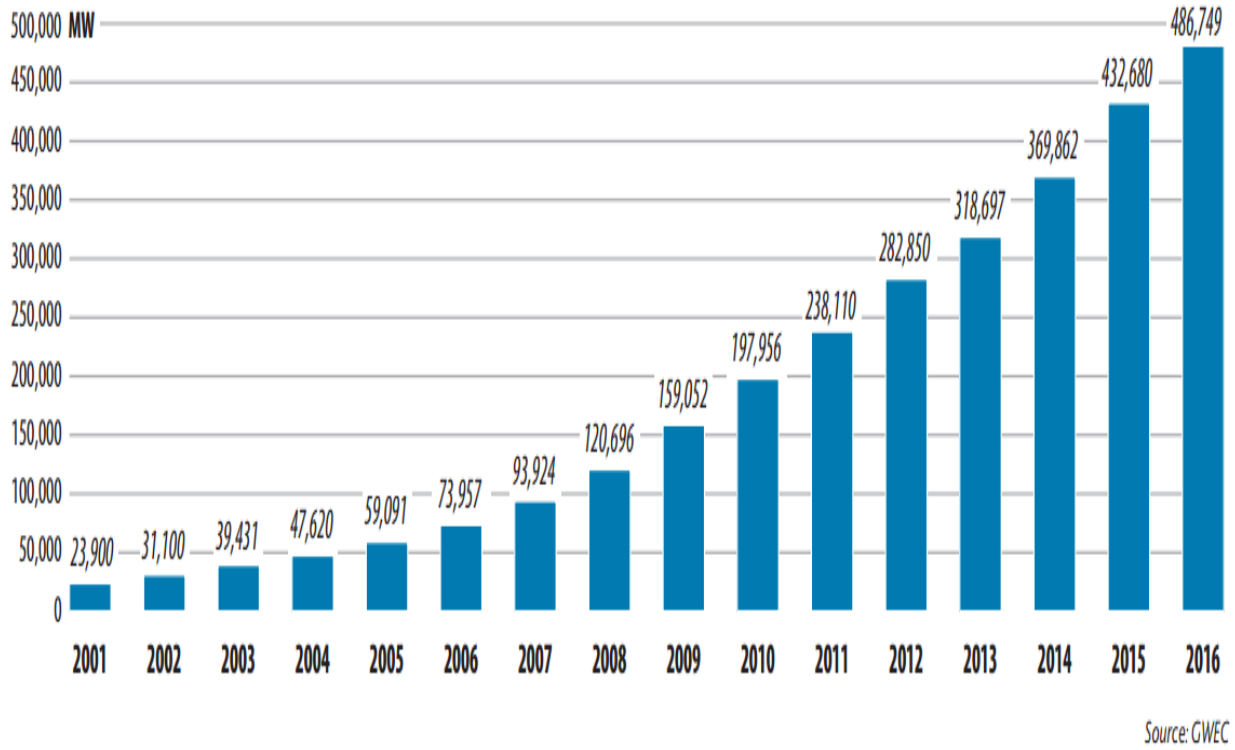

Figure 2: The global accumulative installed wind capacity 2001-2016 (GWEC, 2017)

Moreover, the cumulative wind energy capacity of major countries by December 2016 is shown in figure 3.

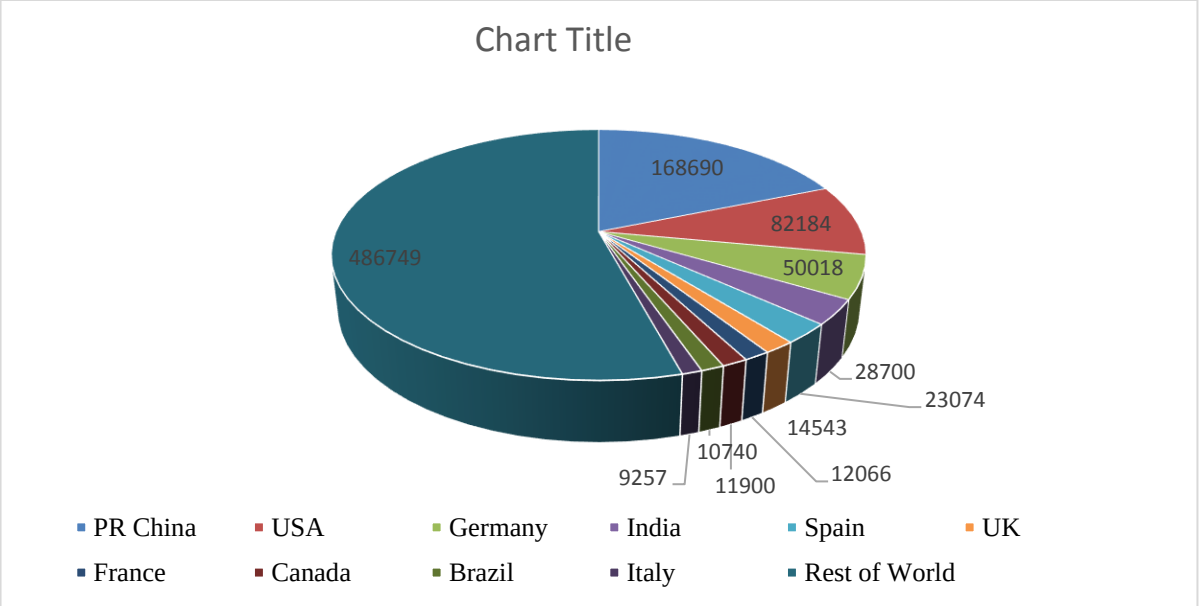

Figure 3: Cumulative wind energy of major countries

From the figure, it is noticeable that the USA is the second country which utilizes highest renewable energy after China. According to the American Wind Energy Association, the current installed capacity of wind energy by the end of 2015 in the US is approximately 73992 MW (U.S. eia, 2016). However, the fact is the availability of wind speed is not same for all places. From the wind maps provided by U.S Department of energy, it can be showed how the wind speed is varied with location and altitude.

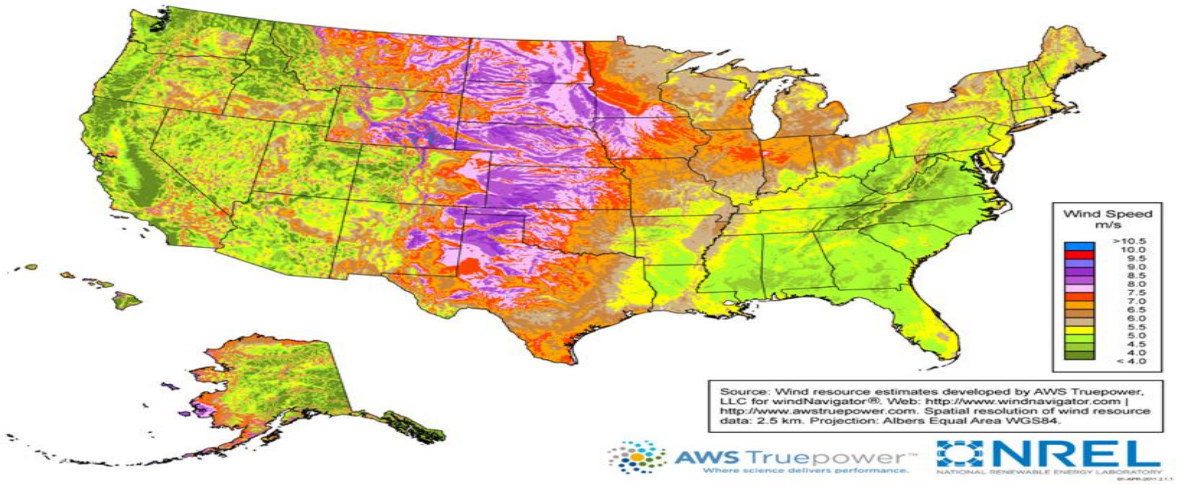

Figure 4: Land-Based Utility 80-Meter Wind Resources Map. (U.S. Energy Department, 2015)

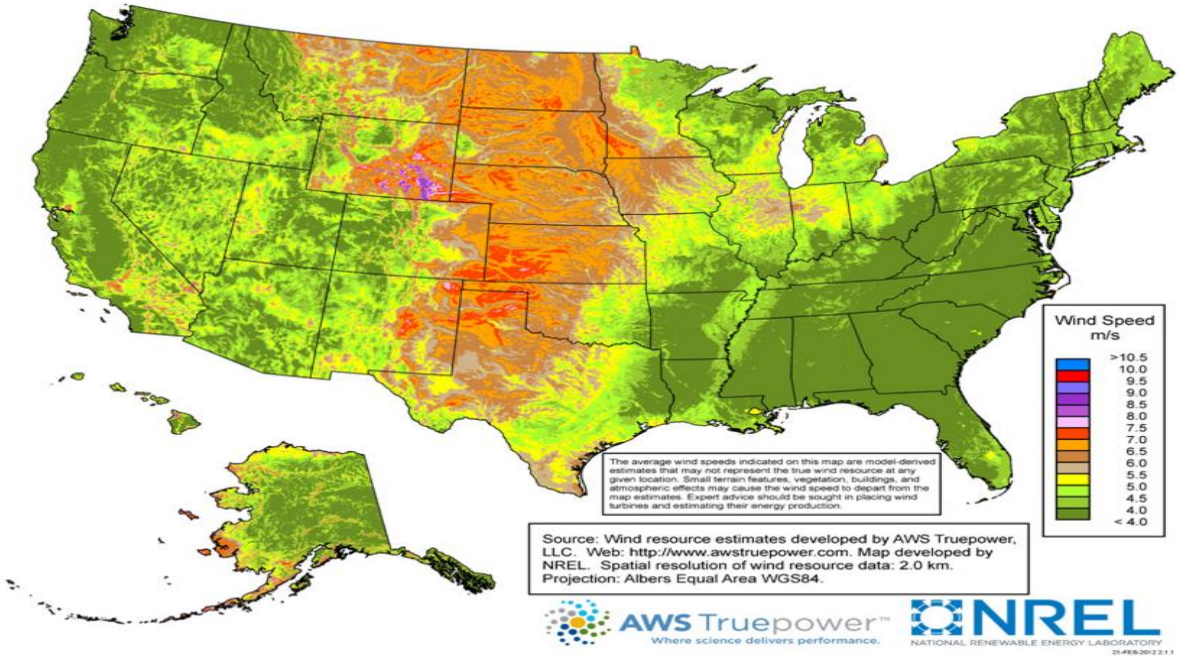

Figure 5: Residential-Scale 30-Meter Wind Resources Map (U.S. Energy Department, 2015)

From figure 4 and figure 5 it is clear that United State has only a few stations where the wind speed is above 8 m/s at an altitude of 80 meters. For elevation, 30-meter majority states have wind speeds below 5 m/s. So, concentration is going to small scale wind. The term small wind is defined as wind operated electric generators with the rated capacities of 100 kilowatts (kW) or less. Moreover, micro wind is a subset of the small wind classification which is defined as turbine with rated capacities less than 1kW (Duffy, 2010).

Nowadays microgeneration is the idea of distributed power generation utilizing sustainable resources that exist in and around the home to produce and store heat and electricity. In general, micro-generation is related with reduced carbon emissions since it doesn't require the utilization of fossil fuels to produce power. Microgeneration technologies incorporate with small scale wind turbines, hydro-electrics, solar systems, biomass sources, and Micro Combined Heat and Power (Micro-CHP) installations. (Duffy, 2010).

Nowadays, Nano grid concept has employed with an independent power source to ensure power quality, peak load minimization, transmission, and distribution losses reduction. Nano grid is defined as a small microgrid, where power network is limited to an individual or a single load. The definition of a Nano grid has established as being 100 kW for grid-tied systems and 5 kW for remote systems which is not interconnected to a utility grid. Small wind turbines or wind energy systems can be integrated with Nano grid to utilize On-grid and off-grid applications (El-Shahat, 2016). It is regarded that small wind turbines will have a significant role in power distribution network. With the development of smart grid concept wind turbine integration could be a viable part of the smart power network.

Although traditional wind turbines are main sources of wind energy, the efficiency of wind turbines decreases with their size. Moreover, the losses due to friction in the rotating components such as bearings causes reduction of efficiency. The wind turbine blade also suffers from fatigue and wear due to the rough weather. Furthermore, the questions arise about installment cost, spaces, maintenance cost, bird issues, sound pollution and environment pollution. These drawbacks of wind turbines urge emergence of a new concept of wind energy harvesting. The energy harvesting can be obtained from flow induced vibration of vortex blade-less wind generators. So, along with the design and performance analysis of small wind turbines, this work also investigated the possible extraction of power from wind energy by using a new conceptual vortex bladeless wind generator. This kind of wind generator can also be used as reliable power sources in Nano grid.

To ensure a reliable source of energy and smooth running system the first and foremost step is to build up a complete model where all components are integrated according to their linkage. It is a great challenge for a wind turbine to do this experimentally in the practical environment by trial and error method. Rather, it is good practice to analyze the system by a well-established

computational method. In this study, the main focus is to design a small scale wind turbine blade model, performance test of that model and further analysis of the modern small-scale wind energy system. There are two types of horizontal axis wind turbine blades were designed by considering all aerodynamic characteristics. After that performance analysis was done by BEM and CFD method. A new conceptual blade less wind turbine model was also developed to find out the potentiality of small wind.

1.2 Wind Energy History:

The usage of wind energy is one of the oldest technologies in the world. The first historical reference was found from Hero of Alexandria in the first century A.D. In his work Pneumatics, he described a device which supplied air to an organ using wind mill [1]. The next reference is from Al Masudi's report. The report described that vertical rotor axis windmills were used in Persian in 9^{th} century A.D. Those are drag type windmills which were called Seitan wind mills (Vowles, Early evolution of power engineering, 1932). The first appearance of wind mills in Europe happened in the 12^{th} century. Though the European wind turbine had some influence from Seistan windmills, the northern European windmills were horizontal axis and lift force driven type. In northern Europe, the wind energy was primarily utilized for applications such as pumping water, grinding grain, sawing wood, and so on. These mills had four blades. Before the industrial revolution, these windmills were one of the primary sources of energy. However, after the revolution theses type of wind mills were disappeared due to their non-dispatch ability and non-transportability (Vowles, 1930).

Figure 6: The ancient Post Mill (http://en.wikipedia.org/wiki/File:Oldland_Mill.jpg)

However, the continuous revolution in wind sector was going on in Europe. The European wind turbine had found with sophisticated design on an early 19th century. European stock type wind turbine had yaw mechanism containing manually operated yaw rotors. The blade had cross-section was designed by airfoil shape including twist angle. The output power of turbine also could be controlled automatically (Hills, 1994).

Beside the European, a different type windmill was used throughout the United States on 19th century. This type of technology had distinctive features such as the multiple blades and regulating systems. This type of wind mill was often called as "fan mills." The integral automatic part of the modern wind turbine came from the regulating system of windmills.

Figure 7: American windmill for water pumping (US Department of Agriculture)

The era of electricity generation by wind began close to 1900's. Initially modern wind Turbine for electricity generation was constructed in Denmark in 1890. During the same time, a large wind turbine with 17 m picket fence rotor was made in Cleveland, Ohio. This turbine was introduced by Charles Brush in 1888. In the following years, small-scale wind generation started to move forward. The most notable pioneer of the small scale was Marcellus Jacob. The feature of Jacobs wind turbine was three blades. This types of turbine had true airfoil shapes which was the pioneer of modern small-scale wind turbine design. However, the outstanding feature of Jacobs wind turbine was it could intergrade with residential storage power system and battery storage system (Jacobs., 1961). In the United States, a large turbine with two blades and 53.3 m diameter was developed by Smith-Putnam in 1948. The power rating of this turbine is 1.25 MW. Unfortunately, this wind turbine was too large for that time wind energy technology, and blade failure occurred in 1945 (Putnam, 1948). At the late of the 1960s, the environmental consciousness was getting interested due to the industrialization. The danger of the nuclear energy was also coming in the front of the world in that time. To take the initiative in renewable energy development along with the NASA, the US Department of Energy (DOE) sponsored in different projects in wind

technology. Most of the projects were allocated for large scale of wind energy. California is a remarkable place in the United States for large wind energy development. In recent years, the large wind turbine capacity increased from 25 kW to 6 MW (Manwell & McGowan, 2009) . Figure 8 shows the evaluation of typical commercial wind turbine size in recent years.

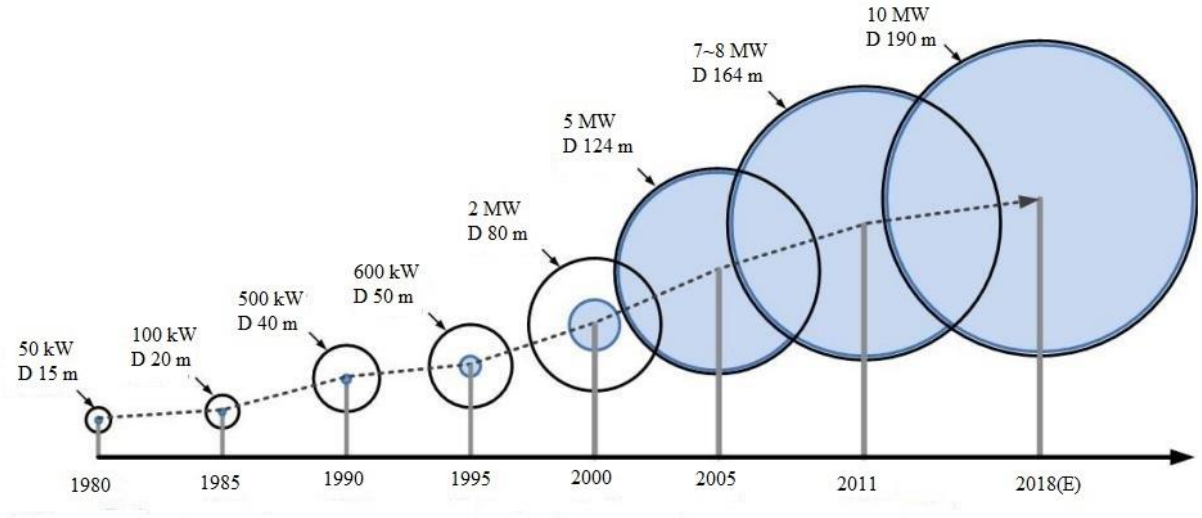

Figure 8: The modification of wind turbines sizes with time being (Steve Connors, MIT)

However, DOE also supported some scale wind turbine building and test facilities in Colorado. Some remarkable designs of the wind turbine such as Darrius turbine, Savonius rotor, were experimented step by step. The contribution of different part of science and technology such as material science, power electronics, aerodynamics, control system, analytical design and so on is increasing on wind energy sector day by day. Some advanced concepts like the vortex turbine, , Musgrove rotor, diffuser augmented design etc. were also suggested by time being. However, among all the turbine technologies, the horizontal axis wind turbine design was found most efficient and popular (Mathew S. , 2006).

1.3 Wind Turbine Theory

1.3.1Wind Turbine

The fundamental idea of a wind turbine system is to convert the kinetic energy of the moving air into mechanical energy and at last into an electrical energy with the application of an electrical generator. Wind turbines come in many shapes and sizes relying upon the environmental location in which it is expected to operate. There are two main categories of wind turbines. One is Horizontal Axis Wind Turbine (HAWT) and another is Vertical Axis Wind Turbine (VAWT).

1.3.2 Horizontal Axis Wind Turbine (HAWT)

Horizontal axis wind turbines are defined as those turbines in which rotational axises are parallel to the direction of free stream flow. This kind of wind turbines operates on the basic principle of lift. Turbine blades are made by airfoil geometry where the upper surface of this geometry is fairly rounded as the lower surface is comparatively flat. When air travels over turbine blade, the two most important aerodynamic forces named as lift and drag. Lift force acts perpendicular direction where drag force acts parallel direction of the wind flow. Due to the pressure difference between the top and bottom surface of the wind turbine blade, the torque is generated which rotates the turbine. Figure 9 shows the main principle of horizontal axis wind turbine operation.

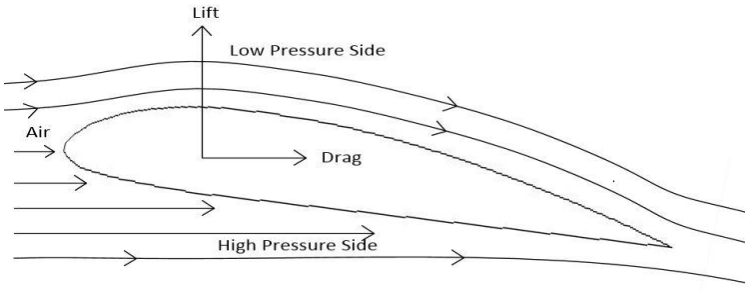

Figure 9: Basic Principle of Horizontal Axis Wind Turbine operation

1.3.3 Vertical Axis Wind Turbine (VAWT)

In vertical axis wind turbine (VAWT) the rotational axis is perpendicular to the direction of the air stream flow. VAWT are classified as into different categories such as Savonius, Darrieus H-rotor. Savonius wind turbines work using the principles of drag whereas Darrieus and H-rotor wind turbines run mainly on the principle of lift. Figure 10 shows different types of the vertical axis wind turbine.

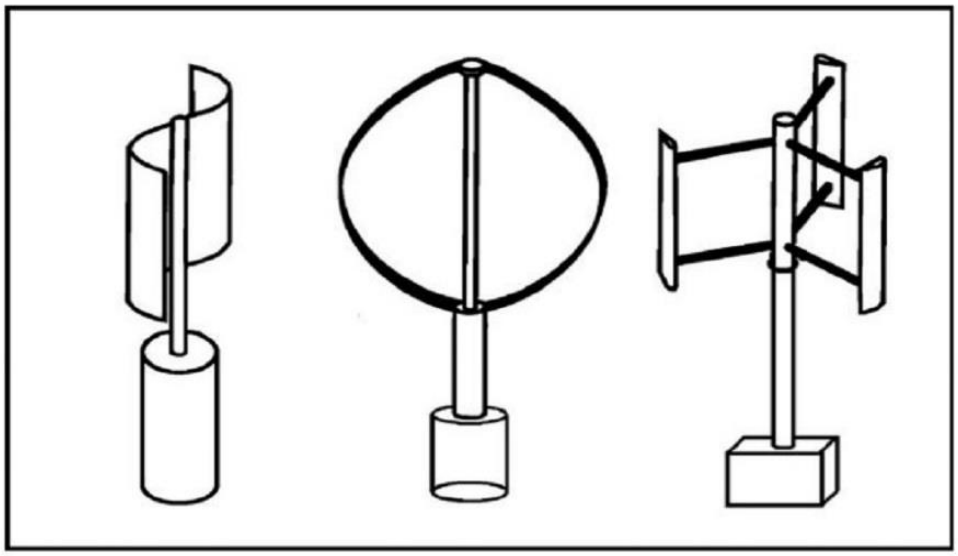

Figure 10: To left is a saponins turbine, in the middle Darrieus turbine and to the right H-rotor (S. Eriksson, 2008)

1.3.4 Comparison between HAWT and VAWT`

Horizontal axis wind turbines (HWT) are considered more efficient in operation than vertical axis wind turbines (VAWT). However, VAWTs are independent with wind direction. They do not need yaw arrangement, pitch control or gear mechanism. There are few movable parts in VAWT which lead lower maintenance efforts and costs (Davood Saeidi, 2013). The VAWT machinery has some special features which make it suitable for the applications in small scale, especially in complex circumstances such as urban areas with tall buildings roof top and structures. It is declared that the reliability of VAWT can be improved when it deals with low blade speed (Joshua Yen, 2012).

However one of the common disadvantages of VAWTs is that they must be installed adjacent to the ground level where the air velocity is relatively low. And this low air velocity leads very low efficiency. Another disadvantage is for larger VAWTs, is the greater expenditure of material per square meter of the surface covered in comparison to installations of HAWT. However, HAWTs have gained much attention from research and commercial sectors as they have higher efficiency than vertical axis wind. Horizontal axis wind turbines have advantage of low cut-in wind speed. In over-all, they have relatively high coefficient of power (Patel Hardik, 2013). HAWTs have some limitations too. They need yaw mechanism to adjust the turbine towards the wind. Since the wind naturally blows more vigorously and evenly at greater heights, horizontal axis wind turbine must be installed on the tower. The generator and gear transmission of these types of turbines are required to be placed on the tower which makes the whole system more sophisticated. Usually, wind firms are used a large wind turbine to generate power commercially (Luisa C. Pagnini, 2015). Figure 11 shows the two comparative models of horizontal and vertical axis wind turbine.

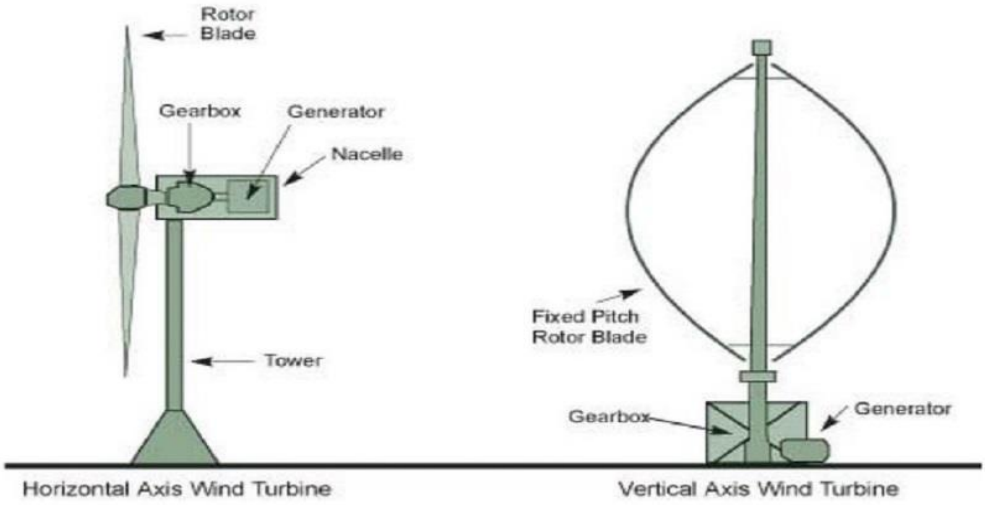

Figure 11: To the left horizontal axis e and the right vertical axis wind turbine (Salih, 2014)

1.3.5 Small Scale Wind Turbine and Scope of Small Wind

Nowadays, a wind turbine is designed, for both large and small scale, according to the application field. There are numerous definitions of a small-scale wind turbine. The most important international standardization organization, the IEC, defines SSWTs in standard IEC 61400-2 as the wind turbines having a rotor swept area of less than 200 m^2, equating to a rated power of approximately 50 kW generating at a voltage below 1000 V AC or 1500 V DC (WWEA , 2015) . Moreover, small scale wind turbines are classified as micro (1 kW), mid-range (5 kW) and mini wind turbine (20kW+) (Simona Culotta, 2015). Due to the flexibility of installation and to catch up the world's small-scale wind potential small scale wind turbines are getting more popular. From the world small wind report,2015 it is showed that by the end of 2013, a cumulative total of at least 870'000 small wind turbines were installed all over the world. Regarding install capacity China, USA, UK is in leading position. Their percentages of the global capacity are 41%, 30% and 15% correspondingly (WWEA , 2015).

CHAPTER 2

LITERATURE REVIEW

Strenuous exploration is continuously offered for the advancement of wind turbine technology. As renewable energy was growing in interest, the development of wind technology spread throughout the world in the last decades. Among all types of wind turbines, horizontal axis wind turbines have gained interest due to their high performance. Beside that, to lessen the drawbacks of bladed wind turbines, a bladeless concept has also been introduced

2.1 Horizontal Axis Wind Turbine Blade Design Approach

Wind turbine design and performance analysis are continuous work. For horizontal axis wind turbines the most significant part is blade geometry. For small scale, various types of blade geometry were developed where, sometimes blade cross-sections are made by the airfoil, sometimes not. Hirahara, Hiroyuki et al. developed and tested very small wind turbine of 500 mm rotor diameter. As the size of the turbine is very small, the blade is designed for fan type instead of taper blade. The cross-section of the blade is followed by NACA 2404 template. Experimentally, the rated power coefficient of this turbine was 0.35 and optimum driving condition to speed ratio is 2.7 (Hiroyuki Hirahara, 2005). As this kind of micro wind turbine has small power capacity, there will be needed more than one wind turbine to fulfill power requirement for a small unit like household activities. Rather than that, it could be possible to enhance capacity by increasing diameter of the turbine but still in small range. Goundar et al. designed a three bladed 10 m diameter tidal Horizontal Axis Turbine and then predicted the performance using BEM method. This turbine had tip speed ratio 4, and the maximum efficiency was 47.6% with the 2 m/s wind speed (Jai N. Goundar, 2013). Watanabe et al. concentrated on optimum design of small

HAWT blade shape operating in low Reynold number. In this work coefficient of performance is predicted by BEM where three-dimensional blade shape is directly provided. Here the performance improvement is 4% compared to the experimental wind tunnel data (Yukio Watanabe, 2007). It is clear that with low wind velocity and small radius the power output of the wind turbine is very low which is not usable in daily household activities. Moreover, the performance of small wind turbines is also very poor. So concentration goes to other parameters such as Reynold number, airfoil design, and selection. Ronit et al. designed a special airfoil for low Reynold number which is used a two-bladed wind turbine. Here the coefficient of performance is 0.255 at height 8.22 m at air velocity of 6 m/s and pitch angle 18 degrees (Ronit K Singh, 2013).

2.2 Blade Element Momentum (BEM) Analysis Development

Performance analysis and blade design are connected to each other. For performance prediction Blade Element Moment (BEM) based analysis is considered as most acceptable and efficient one. Various codes and algorithm have been established to determine optimum chord and twist distribution, and to predict performance. The remarkable BEM based codes are Aerodyne (Hansen, 2005), WT_Pref, etc. There are also many types of research that have been done on BEM. Vitale introduced a code to get optimum blade design and efficiency (A. j. Vitale, 2008). BEM method is a combination of Momentum and Blade Element Theory. In this method, the turbine blade is divided into the small annular segment. Then one-dimensional linear momentum conservation is applied to the segments. After that, the forces, torque as well as power are calculated for each segment based on the sectional aerodynamics characteristics. In BEM the most significant parameters are induction factors and aerodynamic characteristics. Although BEM is well known and very efficient model for power prediction, it also has some limitations. In the case of wake

turbulence and turbine blade stall condition BEM cannot calculate the accurate values of performance parameters. So wake and stall correction were introduced.

2.2.1Wake Correction:

In momentum theory, the momentum in air flow changes due to the thrust on the body or blade. However, in a real scenario, the downstream flow of the turbine expands suddenly. As well as the turbulence also creates at downstream flow. The momentum theory cannot describe this expansion and turbulence (Manwell & McGowan, 2009). As described before in momentum theory, the flow velocity in downstream is$U(1-2a)$. Where U is considered as upstream velocity, a is axial induction factor. The velocity of far downstream becomes negative when a≥0.5 which is not correct. So, BEM model fails for heavy –loaded condition. Several empirical models have developed to correct the BEM method.

- Spera introduced a model which establishes a linear relationship between thrust coefficient and axial induction factor for the above values of critical point 0.2.

$$\boldsymbol{C_T = 4[a_c^2 + (1-2a_c)a],} \quad \boldsymbol{a \geq a_c = 0.2} \tag{3. 1}$$

  Where a is the axial induction factor, a_c is critical axial induction factor, and C_T is the thrust coefficient (Crawford, 2006).

- Buhl determined another empirical correction model incorporate with the Prandtl tip-hub loss (Marshall, 2005).

$$\boldsymbol{C_T = \frac{8}{9} + \left(4F - \frac{40}{9}\right)a + \left(\frac{50}{9} - 4F\right)a^2}, a \geq 0.4 \tag{3. 2}$$

- AeroDyn developed correction model which is similar to the Glauert model.

$$\boldsymbol{a = \frac{18F-20-3\sqrt{C_T(50-36F)+12F(3F-4)}}{36F-50}}, \boldsymbol{C_T} > 0.96F \tag{3. 3}$$

- According to the experimental data, Glauert proposed a correction model. Due to the pressure difference between suction side and pressure side flow slips happen at the tip

and hub of the wind turbine blade. Due to this reason, Prandtl introduced tip-hub loss correction model. And Glauert considered Prandtl correction in his model (Manwell & McGowan, 2009).

$$\boldsymbol{a = \left(\frac{1}{F}\right)\left[0.143 + \sqrt{0.0203 - 0.6427(0.889 - C_T)}\right], a > 0.4} \quad (3.4)$$

Where a is the axial induction factor, C_T is the coefficient of thrust, $F = F_t.F_h$ is the multiple of hub and tip loss factor.

$$\boldsymbol{F_t = 2arcos(e^{\frac{Z(R-r)}{2Rsin\phi}})/\pi} \quad (3.5)$$

$$\boldsymbol{F_h = 2arcos(e^{\frac{Z(r-r_h)}{2Rsin\phi}})/\pi} \quad (3.6)$$

In this work, Glauert wake model was applied for predicting coefficient of performance.

2.2.2 Stall Correction

In blade element momentum (BEM) method, the coefficient of lift and coefficient of drag are needed to predict power in every blade segment. For the convergence of induction factor lift and drag, coefficients are needed at a high angle of attack range. The coefficient of lift and drag from wind tunnel test have limited range. For this reason, it was needed to develop a universal model of the coefficient of lift and drag. Lanzafame introduced a model for representing the coefficient of lift and drag (R. Lanzafame, 2007). Tangler made a global stall model for aerodynamic characteristics prediction based on flat plate theory for airfoil (Jmaes Tangler, 2004). According to him, the coefficient of lift and drag are defined as.

$$C_L = 2sin\alpha cos\alpha \quad (3.7)$$

$$C_D = 2sin^2\alpha \quad (3.8)$$

Here, α is the angle of attack.

In this work XFOIL software was used to determine coefficient of lift and drag for specific airfoil. It is noticeable that depending on this 2D generated data the complex 3D flow on turbine blade

region couldn't be simulated perfectly by BEM. The pressure distribution on rotational blade surface is different from steady 2D airfoil pressure distribution. In real cases the lift and drag values are higher than the 2D aerodynamic data. This behaviour of flow leads stall-delay phenomena (D. Hu, 2006). Therefore, for including stall delay in BEM, several correction methods were developed. An empirical correction of lift coefficient was introduced by Snel (Breton.S.P., 2008). He corrected only lift drag force. After that Du-Selig combined the snail model and experimental wind tunnel data to develop the Du-Selig model (Du.Z & Selig.M.A, 1998). Another correction was done based on pressure distribution by Bak (C. Bak, 2006). The most updated and popular correction model was introduced by Viterna and Corrigan (Jmaes Tangler, 2004). This correction method is most suitable for fixed pitch wind turbines. In this study Viterna and Corrigan correction model was used to modify the BEM.

2.3 Computational Fluid Dynamics (CFD) Analysis of Wind Turbine Blade

However, for the time being it was realised that the real 3D steady and unsteady flow impact should also need to be considered to get the accurate efficiency of the turbine. Moreover, in BEM interaction between annular blade elements is not considered. But in real time operation of wind turbines the flows in different annular tubes interact which needs to be considered as spanwise interaction. In BEM method 2D aerodynamic characteristics are used to determine the coefficient of lift and drag. So BEM cannot simulate the complex 3D flow. However, it is needed to consider rotating frame and centrifugal forces along the blade span to get accurate efficiency. Considering all disadvantages of BEM, with the advancement of computational research Computational Fluid Dynamics (CFD) based approach has got focus recently. In CFD the mathematical model is developed based on the continuity, energy conservation and momentum equations. Nevier stocks equation is the governing equation of CFD model. Viscosity and turbulence models are also

integrated according to the problem statement. There are three main steps to complete the whole task in CFD. These are pre-processing, solving, and post-processing. The performance prediction of wind turbines using 3D CFD method is a very complex analysis. Direct numerical simulation (DNS) has some limitation due to the nonlinear behaviour of the Navier-Stokes equations. Before computing in CFD the turbine blades need to model according to the optimum dimensions of chord length and twist angle. One of the challenges of the wind turbine CFD simulation is to identify the perfect boundary conditions for complex blade geometry. A good quality of meshing is another key point of simulation success. However, several turbulence models were introduced for wind turbine analysis such as k-epsilon model, Spalart-Model, SST model and so on (ANSYS Inc, 2009). Among all turbulence models k-omega SST model has better agreement for the performance analysis of small-scale wind turbines. Khchine and Sriti used CFD for calculating aerodynamic characteristics of airfoil S809. Then based on those aerodynamic coefficients, they implemented BEM to predict the performance of HAWT (Mohammad Sriti, 2016). Amano and Malloy have done their research on CFD analysis of straight span-wise and swept wind turbine blade. Though, the straight commercial blades were found very efficient at lower wind speed, from the pressure contour results they concluded that swept edge blades could generate more power than straight span blades (R. S. Amano, 2009). Keerthana et al. have concentrated on the aerodynamic analysis of 3 kW small scale HAWT by CFD. They first configured the turbine rotor by BEM. After that, normal force, torque and power were investigated by varying wind speed at Tip speed ratio 6. From their analysis, the maximum power has been obtained at Tip speed ratio 5.8. Moreover, Flow field observation was also done. They concluded that flow separation occurred at wind speed 3 m/s and 4 m/s led the lower values of normal force and torque (M. Keerthana, 2012). Another investigation on BEM and CFD of HAWT was done by Dimitriadis at

el: Initially, they compared between XFOIL results and CFD results for the coefficient of lift and drag. They have got that XFOIL tends to overestimate of lift coefficients values. They also proved that the SST turbulence model was more accurate than RSM turbulence model. Finally, they ended up with the comparison of power coefficient between BEM and CFD. The authors got maximum power coefficient 0.48 by BEM and 0.42 by CFD tip speed ratio 7 (E. Dimitriadis, 2014). Emam and et al. also made the comparison between analytical method and numerical method for performance prediction of HAWT: They also compared the results of these methods with experimental data. Some induction factor correction models in BEM were introduced in their work. The comparison was made for power coefficient and as well as for thrust coefficient. The CFD results were found to be more agreeable with the experimental values. On the other hand, among all BEM methods, Wilson correction model gave a close match with the measured values. The air velocity streamlines at flow visualization were also investigated in that study (M. K. Emam, 2015). However, this running work investigated the simulated performances of small scale wind turbine blades, which was made by mixed airfoils. Here, the turbine blade was designed for small scale wind energy. The turbine blade design was performed before the performance analysis and flow visualization. Then the comparison between results which were gotten from BEM and CFD methods was made for the further analysis.

2.4 Vortex Bladeless Wind Generator Concept Development

The operation principle of vortex wind generator is different from the conventional lift type horizontal axis wind turbine. As fluid flows over bluff bodies with a specific velocity range, vortex shedding is created at the trailing edge of the bluff bodies. The shedding of the vortices will lead to vibration in the bluff bodies. And due to the vibration the bodies will oscillate at a specific frequency (Bearman, 1984) (Rostami, 2017). Although vortex bladeless wind turbine is potentially

sound, the design and development of new technology like this needs more research. A Spanish company named vortex, is trying to develop this technology commercially. The vortex bladeless turbine concept came from the Tacoma Narrows Bridge collapse in 1940 in Washington. David Yáñez, one of the vortex company's cofounders, first realize the idea during learning of the collapse of the Tacoma Bridge. The reason behind bridge failure was excessive vibrations formed by the spinning motion of wind. Despite of stating this as engineering failure Yáñez said "This is a very good way to transmit energy from a fluid to a structure". If a vortex were bigger in its shape it could catch more energy from wind. But in the meantime there are some challenges related to fluid mechanics. Instead of cylindrical shape, conical shape (increasing diameter from ground to top) can make the passing air more turbulent. And this turbulence will lead vorticities in fluid and vibration in conical shape (Mckenna, 2015). Gohate et al studied the scope and feasibility of vortex bladeless wind turbines. In their work he made a mathematical model to get natural frequency for a cylindrical body. Here the targeted Reynold number range was from 300 to 300000. The Straul number and wind velocity were 0.2 and 2.88 m/s. In their work, the maximum power extracted from 10 m length turbine is 3.7 kW (Gaurao Gohate, 2016). Harshit at el. concentrated on experimental work on vortex bladeless wind turbines. They made a conical shaped prototype model and tested on practical environment. They integrated classical generator with the vortex generator. The oscillation due to vibration of mast was converted to rotational energy by belt pulley mechanism. The noticeable thing about this work is that the vortex turbine can oscillate any direction according to the air flow direction (Harshith K, 2016). Though belt pulley and gearing mechanism reduced the manufacturing cost of the turbine, the friction losses due to these mechanisms will increase. However in this study the feasibility study of vortex bladeless wind

turbines was made based the Von Karman effect simulation. And this work leads to the fluid structure simulation of vortex bladeless wind generator.

In this chapter, different types research and theory development related to this dissertation was discussed which lead a validate methodology to fulfill the aim of current work.

CHAPTER 3

METHODOLOGY

3.1 Basic Parts of SSHAWT:

Small scale wind turbine components are not as complicated as a large-scale wind turbines. Figure 13 shows the main parts of the small-scale horizontal axis wind turbine system. As this work focuses on fixed pitch, the pitching mechanism and control system is removed from the design consideration. Some small scale wind turbines have drag type blades which utilizes the drag force of air flow. However, in this work, the operating principle is lifted type commercial large wind turbines but in small scale. The blade's cross-sections are made by the airfoil. The tower, yaw, and nacelle were considered as simple structures.

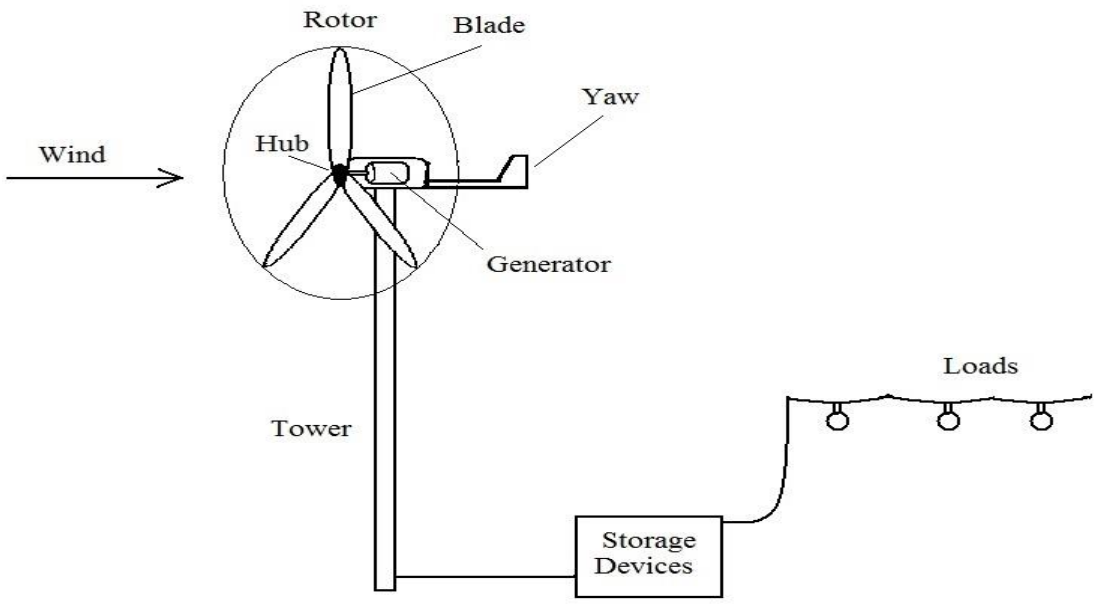

Figure 12: Schematic Diagram of Small Scale Horizontal Axis Wind Turbine.

3.3 SCHAWT Blade Design

In a horizontal axis wind turbine one of the key components is the blade. Usually, large wind turbine blades are made of two or more combinations of an airfoil with variable thickness.

However, in a small scale wind turbine, sometimes one airfoil is enough to build whole blade geometry; sometimes two or more airfoils are used for blade cross-section. However, in design procedure, the main parameters such as wind speed, rotor diameter, airfoil type, and tip speed ratio should be considered first before conducting blade geometry.

3.3.1 Rotor Diameter

The diameter of the wind turbine rotor primarily depends on the expected power and wind condition where the wind turbine will be mounted. The diameter of a small wind turbine is selected in such a way that it will ensure the rotation with low wind speed as well maintain the proper strength of the total structure and blades.

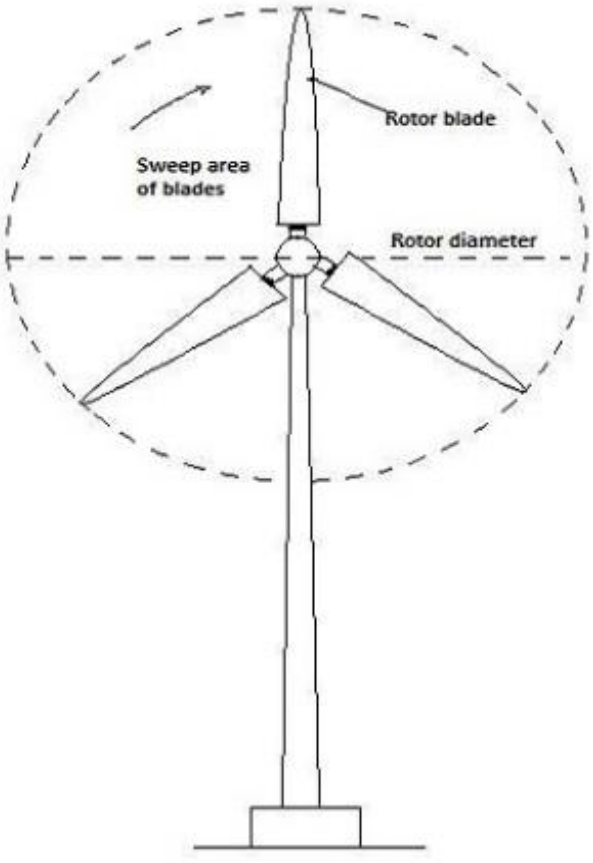

Figure 13: Diameter of wind turbine

At the beginning of design procedure, it is recommended to assume an approximate expected power. From the expected power equation, the radius of the wind turbine can be calculated by equation 3.1.

$$\boldsymbol{R} = [\frac{\boldsymbol{2P_D}}{\boldsymbol{C_{PD}\eta_d\eta_g\rho_a\pi V_D^3}}]^{\frac{1}{2}} \quad (3.1)$$

Where,C_{PD} is the design power coefficient of the rotor, η_d is the drive train efficiency, η_g is the generator efficiency, V_D is the design wind velocity. The design power coefficient C_{PD} range is 0.4 to 0.45. The combined efficiency of generator and drive train is considered 0.9 (Mathew D. S., 2006). The radius of the wind turbine depends on the expected power and wind velocity. By fixing expected power 10 kW the variation of radius with the wind velocity is showed in figure 14.

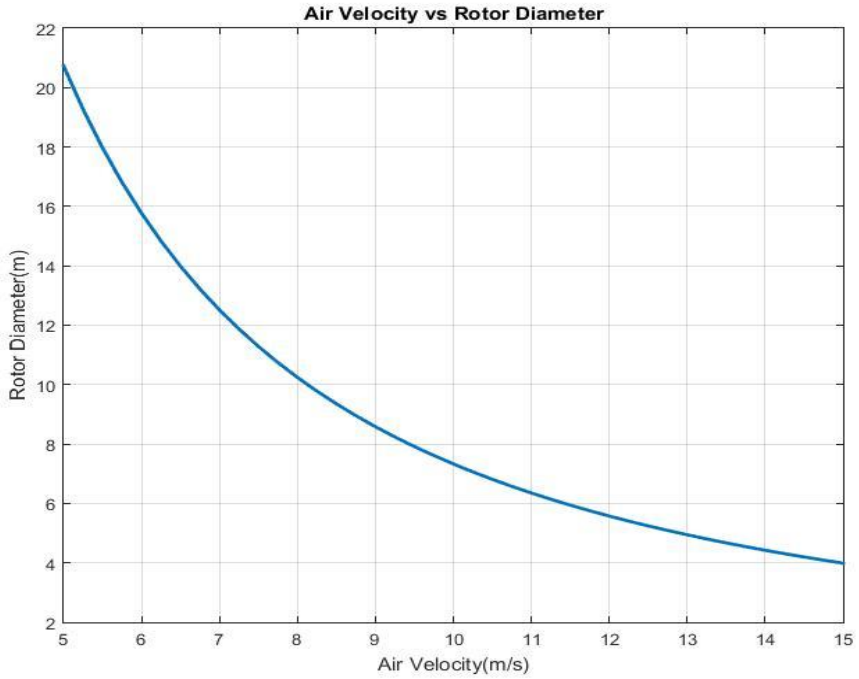

Figure 14: Variation of Rotor Diameter with Air Velocity

3.3.2 Rated and Design Wind Speed

The rated wind speed can be defined as the wind speed when the turbine power reaches to its rated power. On the other hand, design wind speed is another important parameter in which condition

wind turbine power output is maximum. According to IEC61400-2, the design wind speed is 1.4 times of annual mean wind speed (L. Wang R. Q., 2016). As this work focused on variable-speed, the wind turbine was designed to operate at its maximum coefficient of performance from a cut in wind speed to rated wind speed. The designed and rated wind speed was considered as the same which is 7 m/s. From the power equation 3.1, it is showed that the energy of wind is proportional to the cube of the wind speed. However, a higher rated wind speed is not always appropriate for the efficient operation. In this concern, annual power output is vital parameter to make a decision about wind turbine behavior. The annual power output is a function of the local wind speed distribution. It can be described as a Weibull distribution with a shape parameter and scale parameter. The annual power output can be calculated as:

$$P_{annual} = 8760 * \frac{1}{2}\rho A\eta C_{p,o} \int_{cut\ in}^{rated} v^3 f_{rayleigh}(v)dv + 8760 * P \int_{cut\ in}^{cut\ out} f_{Rayleigh}(v)dv \quad (3.2)$$

Where A is wind turbine rotor area,η is efficiency including mechanical and electrical efficiency, $C_{p,o}$is the maximum power coefficient of the blade, $f_{Reliegh}\,(v)$and is the Rayleigh wind speed distribution, which is defined as:

$$f_{Reliegh}\,(v) = \frac{\pi}{2}\frac{v}{\overline{v}^2}\exp(-\frac{\pi}{4}\frac{v}{\overline{v}^2}) \quad (3.3)$$

Here $\overline{v}$ is the annual mean wind speed. It was found that lower rated wind speed leads to higher AEP for a fixed pitch variable speed wind turbine (Xinzi Tang, 2009). Usually, wind speed below 2 m/s or 3 m/s are not suitable to produce significant amounts of electricity generation. To design a small wind turbine, it is important to check the availability of wind speed is available at near to the ground level.

3.3.3 Airfoil Selection

Different types of airfoil shapes are available for both traditional aviation and wind turbine technology. With the development of interest in wind energy sector, some dedicated airfoils have

been designed. In case of small wind turbines, the airfoils are not as critical as for large wind turbines. However, there are only a few of airfoil shapes which are suitable for designing small-scale wind turbines. For small scale wind turbines the airfoils should be used at a low angle of attack, where the coefficient of drag is much lower as compared to the lift coefficient. Traditional NACA series airfoils were developed for aviation technology, but nowadays some NACA series airfoils are also used for wind turbine blades. The S8 series airfoils, which were designed by National Renewable Energy Laboratory (NREL) in the USA, are popular in stall-regulated wind turbine blades due to their gentle stall condition (Somers D. M., 2005). The FFA W series airfoil was developed in Sweden. These airfoils were initially designed for large wind turbines such 45 m diameter rotor size. For low Reynold number, Risø series from Denmark are popular (Peter Fuglsang, 2004). Another popular airfoil series is DU series. These were designed in the Netherland are popular in middle and high Reynolds number (W.A. Timmer, 2003). Some special types of airfoils such as SG605X series were designed by Selig/Gigere from the University of Illinois at Urbana-Champaign. These airfoils are popular due to their high lift coefficient and the ability of operation in low Reynold number wind condition which means these airfoils are suitable for a small horizontal axis wind turbine (P. Giguere, 1998).

To select the appropriate airfoil for small wind turbines some parameters should be maintained such as thickness, the coefficient of lift, the coefficient of drag, stiffness in the blade root section, and so on. Usually, the airfoils are tested practically in a wind tunnel within a range of Reynolds numbers and surface conditions. To predict aerodynamic performance, other several software applications are used. In this work XFOIL software was used which is developed according to potential flow techniques. Moreover, CFD is also a popular method of aerodynamic performance analysis. The aim of the aerodynamic analysis is to determine the optimum angle of attack. For the

first part of this work, Airfoil S833 is used to design blade geometry which was invented by NREL. This special kind of airfoil is made for a small-scale wind turbines. Dan M and et al. have investigated different effects such as Reynold Number effect and roughness effect on S833 airfoil. From Pennsylvania State University Low-speed and Low-Turbulence Wind Tunnel test the maximum lift coefficient for the design Reynolds Number of $0.4x10^6$ is estimated to be 1.10. For the same Reynold number condition, the maximum lift coefficient increased one percent from transition free to the fixed condition. On the other hand for the rough condition, this increment was three percent. In summary, the S833 airfoil has achieved a high maximum coefficient of lift and low profile-drag coefficient and this airfoil should reveal docile stall characteristics to meet the design goal. Moreover, the zero-lift pitching-moment coefficient and this airfoil thickness have been fulfilled (Somers D. M., 2005). Figure 15 shows the coordinates and shape of S833 airfoil.

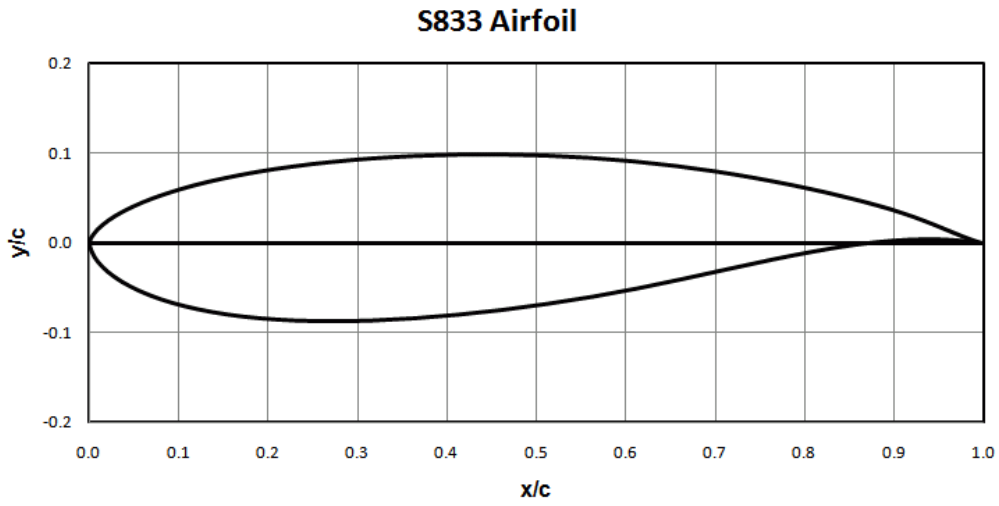

Figure 15: Relative Coordinate of Airfoil S833 (NREL, 2017)

3.3.4 Reynold Number

Reynold number is a very important parameter to determine the wind turbine operating condition and aerodynamic behavior of the wind, The Reynold number is found by using the equation 3.4

given below Where: V_{rel} is the relative wind speed (m/s), c is chord length (m), ν is kinematic viscosity of air ($\nu = 1.511\times10^{-5}$) (m^2/s) at 20^0C.

$$\boldsymbol{Re} = \frac{\boldsymbol{V_{rel}C}}{\boldsymbol{\nu}} \quad (3.4)$$

The small wind turbine typically operates in the wind speed between 5 m/s to 30 m/s. From the analysis of different existing small wind turbine chord distribution, it is clear that the chord distribution varied from 0.05m to 0.5m. It depends on the size of the wind turbine and airfoil specification. Considering all variables, the assumed Reynold number range for a small scale wind turbine is usually between 100000 and 400000 (Lissaman, 1983) (Miley, 1982).

3.3.5 Aerodynamic Characteristics

According to the principle of HAWT operation, the key force to rotate the turbine is lifted force, which is generated by the airfoil cross section. Figure 16 describes these terminologies of airfoils, where φ is a relative angle between air flow stream line and the axis of rotation, α is the angle of attack which is the angle between air flow streamline and chord line, Θ is pitch angle.

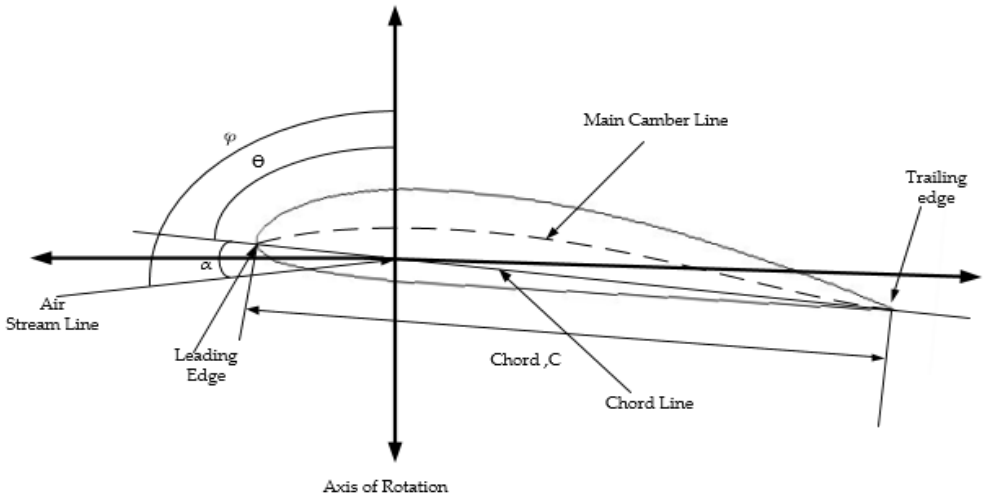

Figure 16: Basic Terms of Airfoil Geometry

To analyze aerodynamic characteristics of the airfoil it first needs the optimum angle of attack. For an initial guess, a 2D polar coordinate XFOIL software is used for the analysis. At the beginning, XFOIL data was compared with experimental wind tunnel data for validation. National Renewable Experiment Laboratory (NREL) Phase VI wind turbine tested data was used as the reference of validation. This wind turbine was developed by National Aeronautics and Space Administration (NASA) for research activities. The blade of Phase VI wind turbine was made by single airfoil (S809). The turbine is stall regulated and pitch is fixed. First of all the coefficient of lift and drag data for S809 airfoil was generated by XFOIL. After that, that data was compared with the experimental aerodynamic data which was measured by Delf University of Technology (TUDelft). Reynold Number was maintained at $1x10^6$ during the experiment. Figure 17, 18 and 19 show the comparison between Xfoil generated data and experimental data for the S809 airfoil.

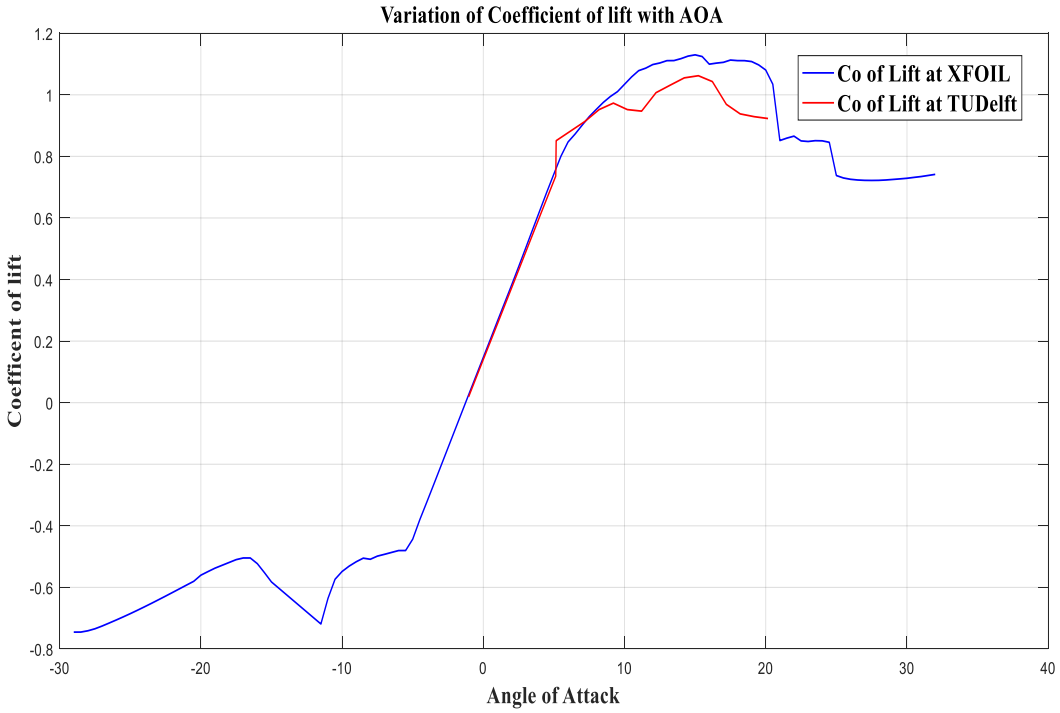

Figure 17: Comparison between XFOIL and Experimental data of Lift Coefficient

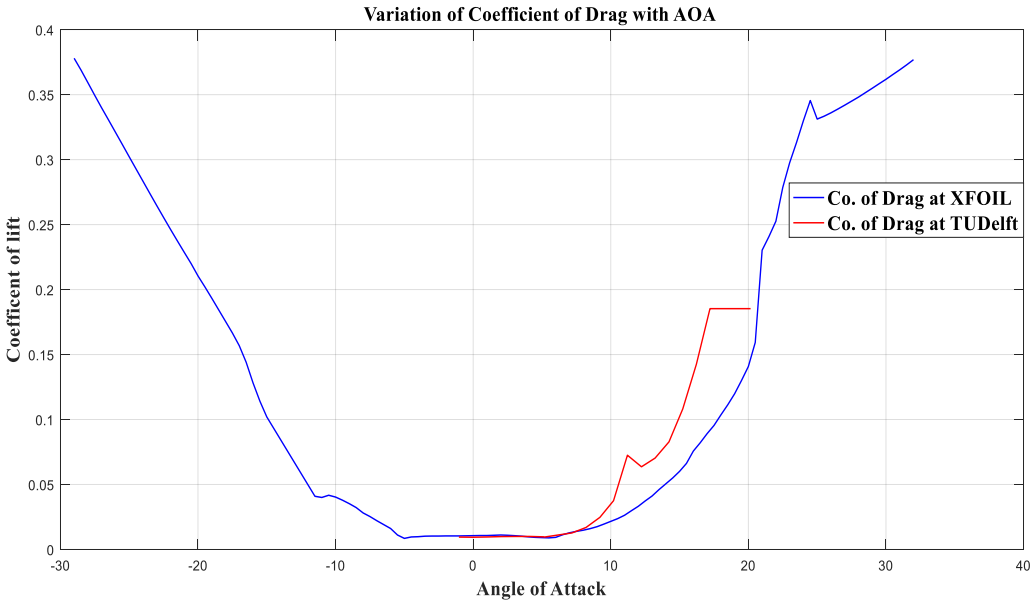

Figure 18: Comparison between XFOIL and Experimental data of Drag Coefficient

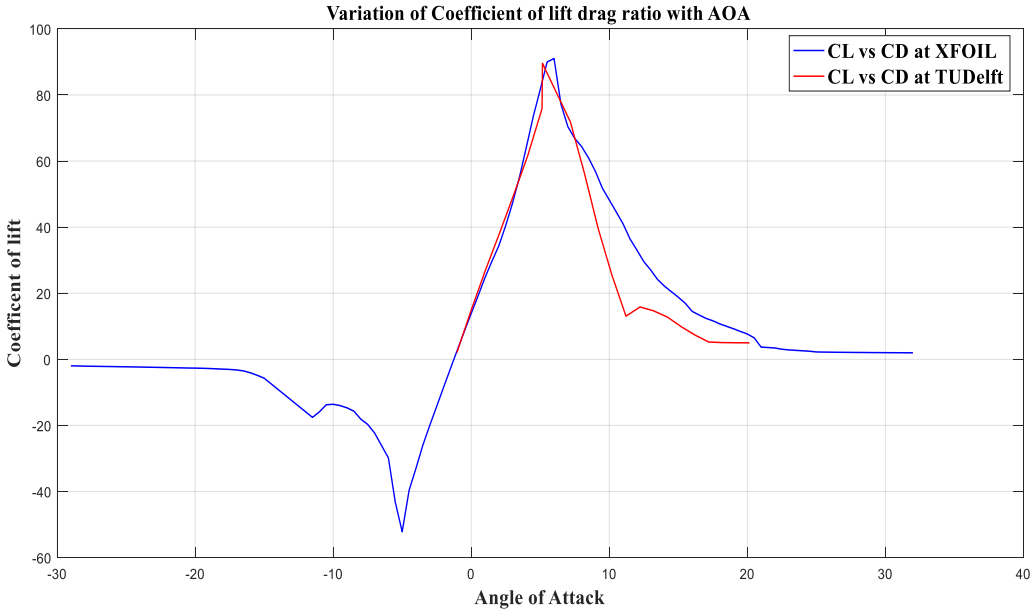

Figure 19: Comparison between XFOIL and Experimental data of Drag Coefficient

From figures 17, 18, 19 it is clear that the XFOIL generated data and the TUDelf University experimental data are close to each other. XFOIL generated data is used for other airfoil's aerodynamic characteristics for further analysis. It is noticeable that for both lift and drag coefficients the XFOIL data fluctuates after the angle of attack 10. This fluctuation can be

neglected for simplification. However, in this current work, S833 airfoil was tested for four different Reynold numbers within the previously selected range. Figure 20 ,21 and 22 represent the aerodynamic characteristics of the S833 airfoil.

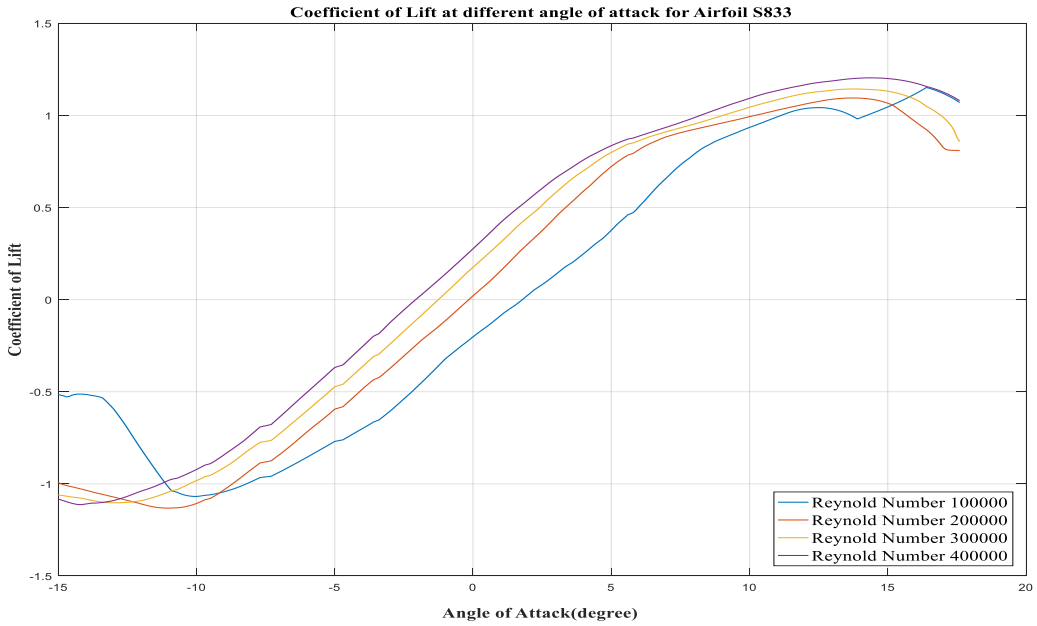

Figure 20: Variation of Coefficient of lift with Angle of Attack

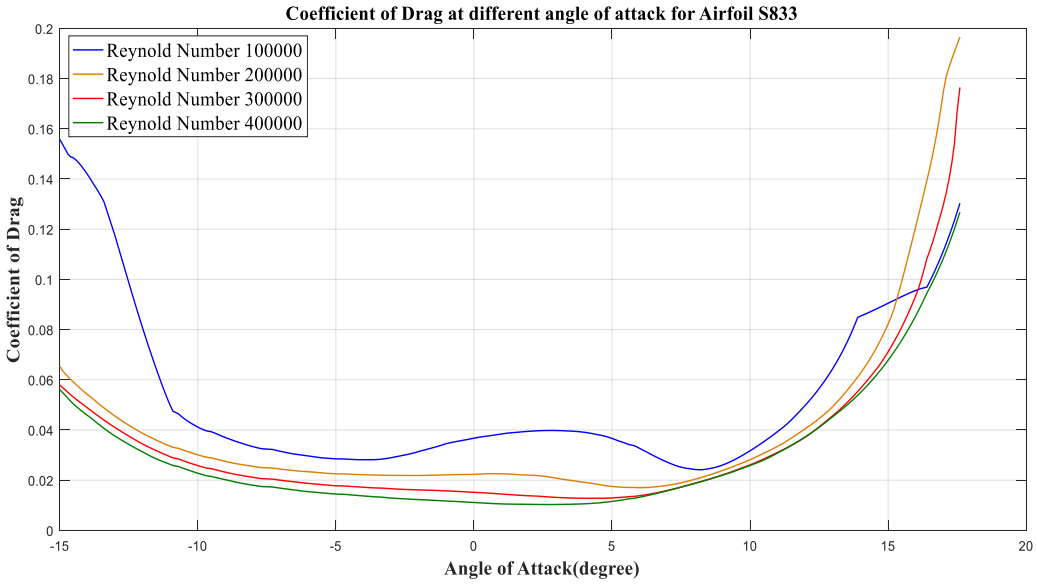

Figure 21: Variation of Coefficient of Drag with Angle of Attack

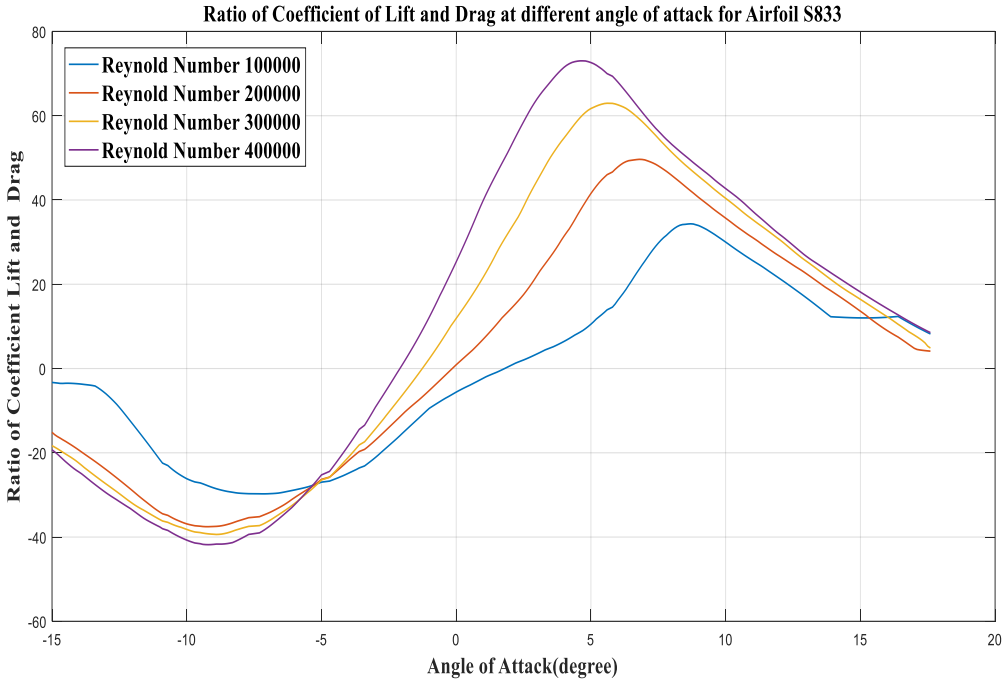

Figure 22: Ratio of coefficient of lift and drag with different Angle of Attack

As this work focused on small-scale wind energy, it recommended considering air velocity is very low. Moreover, considering low wind velocity Reynold number, 200000 is best fit for analysis. At this condition from the figure 20, it is showed that at an angle of attack 7^0, the coefficient of lift is 0.88 which is considered most optimum coefficient for airfoil S833. Another vital parameter is the coefficient of drag. Figure 21 represents the variation of drag coefficient with angle of attack for different Reynold Number. For small scale, lift-type wind turbine coefficient of lift always dominate to the coefficient of drag. The lowest coefficient of drag should be chosen if possible. It is noticed that for the Reynold number 100000 the values of coefficient of drag are higher in comparison to other Reynold numbers. From the curve, for Reynold number 200000 it can be said that the coefficient of drag is very low at an angle of attack 7^0 and the value of the coefficient of drag is 0.01792. Other than two case studies discussed above, figure 22 explains the ratio of coefficient of lift and drag ratio with four smaller scales Reynold number. From the figure above, it is observed that at Reynold number 200000, the pick of the coefficient's ratio is maximum for

the angle of attack 7^0. In summary, the angle of attack 7^0 is the best choice to design a wind turbine blade with S833 airfoil at a low Reynold number.

3.3.6 Tip Speed Ratio

Tip speed ratio is introduced to define the relation between blade angular speed and air velocity; the equation 3.5 defines the tip speed ratio.

$$\boldsymbol{\lambda = \frac{\omega R}{V}} \quad \textbf{(3.5)}$$

Where ω angular velocity of the rotor, R is the radius and V is wind speed.

High tip speed ratio leads to higher rotation of the turbine. When the rotational speed is higher, the efficiency of the turbine is higher and less material is needed to make the blade. For high tip speed ratio, smaller gear boxes are required, but sophisticated airfoil shapes are required. For electrical power generation, the range of the tip speed ratio is $4< \lambda <10$. To determine the optimum value of tip speed ratio, the empirical relation between power coefficient and tip speed ratio was developed initially (Manwell & McGowan, 2009) . After that, a similar procedure to assess optimum tip speed ratio for different airfoils with different blade numbers was developed by Artificial Neural Network. According to that method, the power coefficient is a function of TSR, blade number, and maximum lift/drag ratio (M.A. Yurdusev, 2006).

$$C_p = C_{pSchemitz}\,(1 - \frac{\lambda}{\frac{Cl}{Cd}})(1 - \frac{1.84}{B*\lambda}) \quad (3.6)$$

Here, $C_{pSchemitz}$ is Schmitz power coefficient, which is 0.5926, B is the blade number, Among all the horizontal axis wind turbine the three bladed turbine are mostly balanced and economical for optimum design. And $\frac{Cl}{Cd}$ is the maximum lift to drag ratio. To get the appropriate tip speed ratio figure 24 shows the, relation between coefficient performance and tip speed ratio at different Reynold number.

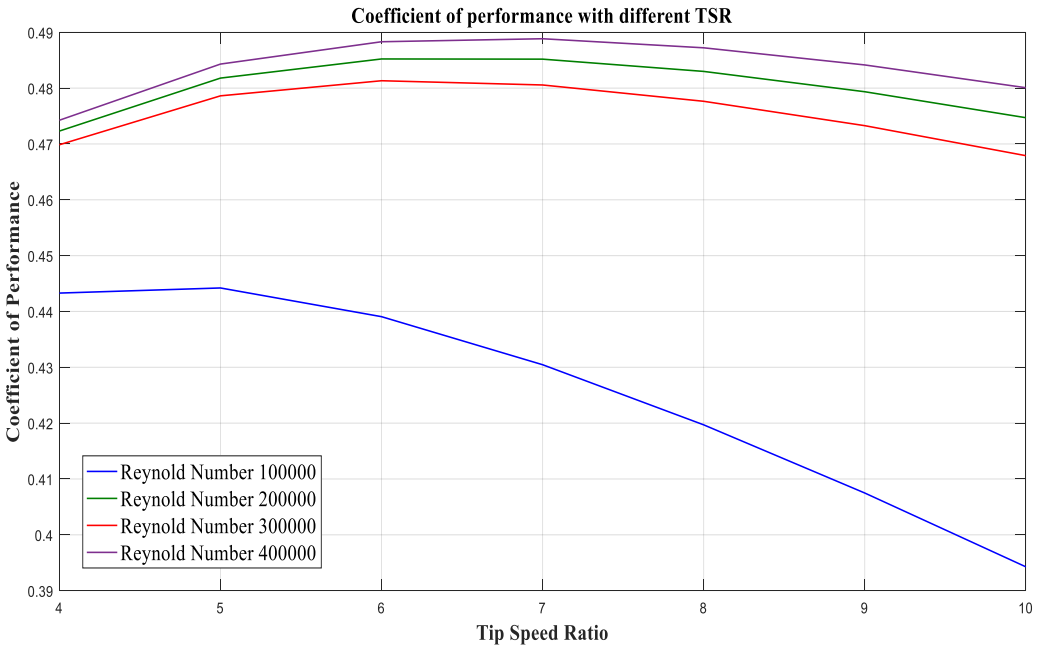

Figure 23: Variation of Coefficient of Performance with TSR at various Reynold Number

From figure 23, the best coefficient of performance is 0.4957 at Tip speed ratio 6.5. Moreover, it is similar to all Reynold numbers mentioned in figure 23. For this tip speed ratio, the blade geometry parameters are selected for further consideration. It is essential to fix whether the turbines operates at a constant rotational speed or variable rotational speed. In case of high tip speed ratio, the geometry of the blade requires slender shape. On the other hand, the low tip speed ratio like this work wind turbine is opposite. It requires a short, thicker blade. Usually, wind turbines cannot always operate at optimum tip speed ratio all the time, but for a range of wind speeds, the turbines operate at different tip speed ratios. If the wind turbine were to operate at a tip speed ratio other than the optimum tip speed ratio, then the performance of the turbine would be significantly less than the optimum performance for which the turbine is designed.

3.4.7 Blade Geometry

An important design feature of a wind turbine is the blade geometry as it is responsible for the extraction of kinetic energy from the wind. Optimizing wind turbine blades is to maximize power

output and efficiency. To determine the distribution of the cross-sectional shape of the blade, some design parameters are required to satisfy the requirements of the BEM theory equation. Once these parameters are selected, it will result in the extrapolation of chord distribution and twist distribution of a blade which closely resembles the Betz limit power production ideal blade. The initial design equation of relative angle and chord for any airfoil can be obtained from the equations 3.7 and 3.8.

$$\boldsymbol{\varphi = \frac{2}{3} tan^{-1}(\frac{R}{\lambda_r})} \tag{3.7}$$

$$\boldsymbol{c = \frac{16\pi r}{BC_l} sin^2(\frac{2}{3} tan^{-1}(\frac{R}{\lambda_r}))} \tag{3.8}$$

Initial values were used to calculate the performance of the turbine by BEM. This an iterative process. Whenever the optimum value of the coefficient of performance comes up for every section of the blade, the associated relative angle and chords were selected as the optimum value. Blade geometry does not only depend on the chord length and twists angle but also the material of the blade. Beside the maintaining aerodynamic characteristics it is also important to ensure the proper strength of the blade. Because of continuous rotation, the wind turbine blade faces cyclic loading and therefore fatigue and crack formation present safety concerns. In most of the cases wind turbine blades face harsh environments, constantly varying wind loads, temperature and humidity changes, erosion, and corrosion. Wind turbine blades should be designed considering all factors. After considering all parameters discussed above, the initial design parameters are given in table1.

Table 1: Initial Blade design parameters

Wind Velocity(m/s)	Diameter (m)	Tip Speed Ratio	Blade Number	Initial AOA	Initial Coefficient of lift	Inner Diameter
7	11	6.5	3	7	0.88	0.2

The wind turbine blade is not uniform throughout the length. The blade was divided into ten segments including the hub section. After applying optimization technique for each section, the

calculated parameters are given in Table 2, where values are dimensionless. By using these dimensionless values, it possible to make wind turbine blade for different diameter.

Table 2: Optimized Blade Geometry Parameters

Blade Segment	Relative Radius	Relative Chord	Relative Angle	AOA	Twist Angle	Power (kW)
1	0	Hub	Hub	Hub	Hub	Hub
2	0.15	0.1974	27.49	4.01	23.48	.2315
3	0.25	0.1591	19.87	5.80	14.07	.568
4	0.35	0.1262	14.76	5.94	8.82	.811
5	0.45	0.1029	11.66	6.07	5.59	1.03
6	0.55	0.0863	9.60	6.19	3.41	1.25
7	0.65	0.0741	8.15	6.27	1.88	1.44
8	0.75	0.0649	7.02	6.29	0.73	1.61
9	0.85	0.0576	6.08	6.24	-0.16	1.71
10	0.95	0.0518	4.69	5.54	-0.85	1.46

The blade segments are divided in such a way that the hub covers 15% of swept radius. However, there is a reference point at the middle of every section. Chords, angles of attack, and twist angles are calculated on these points for all sections. From the chord distribution, it is showed that the maximum chord length is in the second section. After that, the chord length is decreased step by step to the tip of the blade. On the other hand, twist angle is the maximum at the very beginning section close to the hub; after that, values are continuing as decreasing order up to the tip. Figure 24 shows the chord distribution throughout the radius. For manufacturing the blade, sometimes it is needed to linearize the values of chord length.

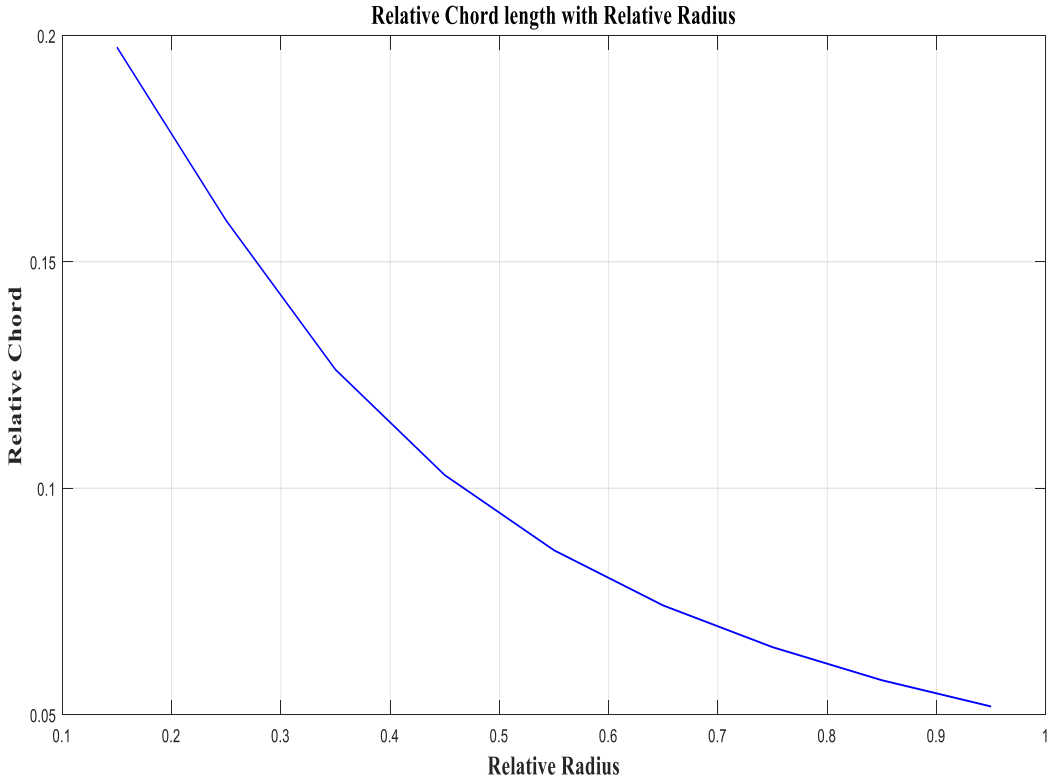

Figure 24: Variation of Relative chord with Relative Radius

3.2 Blade Performance Analysis Using BEM Method

Blade Element Moment (BEM) based approach is the most popular method for performance analysis. This method combines the Momentum theory and Blade Element Theory. Momentum theory is used to determine forces acting on the rotor to produce the motion of the fluid. On the other hand, blade element theory determines the forces on the blade as a result of the motion of the fluid regarding blade geometry. In this method, the wind turbine blades are divided into annular blade elements. After that, one-dimensional linear momentum conservation is applied to all annular elements which leads to the forces and power calculation. These calculations are based on the local aerodynamic characteristics data, the chords, and twist angles of the blade geometry. The airfoil aerodynamic characteristic data such as coefficient of lift and drag is obtained from different

types of polar coordinate software like xfoil. The description of the airfoil aerodynamic characteristics at both low angle of attack and high angle of attack are inevitable in the BEM method. Different lift and drag data directly lead to different power output results. In the iterative procedure of BEM, for every element of the blade, the lift and drag coefficients are expected to have a general mathematical model for a high range angle of attack as well as for a whole range wind speed analysis at yawed or un-yawed conditions. At normal operating conditions such as idling, starting, pre-stall, stall, and deep stall stages the aerodynamic characteristics are also determined from the different angle of attacks. Different types of global stall model for determining the airfoil characteristics are developed. However, sometimes these models are too unpredictable for specific wind turbine airfoil analysis. To characterize "stall delay" phenomena several empirical models have also been developed. Among all of the models, Viterna-Corrigan model is one of the widely used models (Viterna Larry A., 1982). Viterna's equations for the coefficient of lift and drag are as follows:

$$C_l = A_1 \sin(2\alpha) + \frac{A_2 cos^2\alpha}{sin^2\alpha} \tag{3.9}$$

$$C_d = B_1 sin^2\alpha + B_2 cos\alpha \tag{3.10}$$

$$\text{Where } A_1 = \frac{B_1}{2}$$

$$A_2 = (C_L - C_{DMAX} sin\alpha_s cos\alpha_s)\frac{sin\alpha_s}{cos^2\alpha_s} \tag{3.11}$$

$$B_1 = C_{DMAX} \tag{3.12}$$

$$B_2 = C_{D_s} - \frac{C_{DMAX} sin^2\alpha_s}{cos\alpha_s} \tag{3.13}$$

$$C_{DMAX} = 1.11 + 0.18AR \tag{3.14}$$

Here, C_l and C_d are coefficient of lift and drag respectively. And α represents the angle of attack. Another important factor of BEM is induction factor which is described by the axial induced velocity and tangential induced velocity. By using the differential thrust with blade element theory it is possible to determine the axial induction factor

$$C_x = C_l * sin\emptyset - C_d * cos\emptyset \quad (3.15)$$

$$C_y = C_l * cos\emptyset + C_d * sin\emptyset \quad (3.16)$$

$$\frac{a}{a-1} = \frac{\sigma C_y}{4sin^2\emptyset} \quad (3.17)$$

Here, $\emptyset$ is the relative angle and a defined as axial induction factor. However, by using differential torque with angular momentum theory the tangential induction factor a'can be expressed as

$$\frac{a'}{a'+1} = \frac{\sigma C_x}{4\ sin\emptyset\ cos\emptyset} \quad (3.18)$$

Where solidity ratio σ is defined by,

$$\sigma = \frac{cB}{2\pi r} \quad (3.19)$$

Here, c, B, r represent chord length, blade number and local radius of the turbine blade respectively. At the tip of the wind turbine blade, the air flow radially inward direction over the blade tip, creating an obstacle for the circulation of air. This causes reduction of the torque and turbine efficiency. To reduce the loss of torque, Prandtl developed a method to calculate the radial flow effect near the blade tip which is considered much accurate for high tip speed ratios (Wilson, 1976). The Prandtl's factor is defined by

$$F_p = \frac{2}{\pi} cos^{-1}(e^{-f}) \quad (3.20)$$

Where $f = \frac{B}{2}\frac{R-r}{rsin\emptyset}$

Applying Prandtl tip loss correction factor the final two induction factors are expressed as

$$a = \frac{1}{\frac{4F_P sin^2\emptyset}{\sigma C_y}+1} \quad (3.21)$$

$$a' = \frac{1}{\frac{4F_P sin\emptyset cos\emptyset}{\sigma C_x}-1} \quad (3.22)$$

The induction factor getting by Prandtl tip loss correction factor is only accurate for the value less than 0.2. If the induction factor value is greater than 0.2, it needs to use Glaurt average axial interference factor (Wilson, 1976).

$$a = \frac{1}{2}(2 + K(1-2a_c) - \sqrt{(K(1-2a_c)+2)^2 + 4(Ka_c^2 - 1)} \quad (3.23)$$

Where $K = \frac{4Fsin^2\emptyset}{\sigma C_y}$

Whole BEM method is developed by Matlab coding where different segments need different iteration number. The algorithm for the BEM method is given bellow.

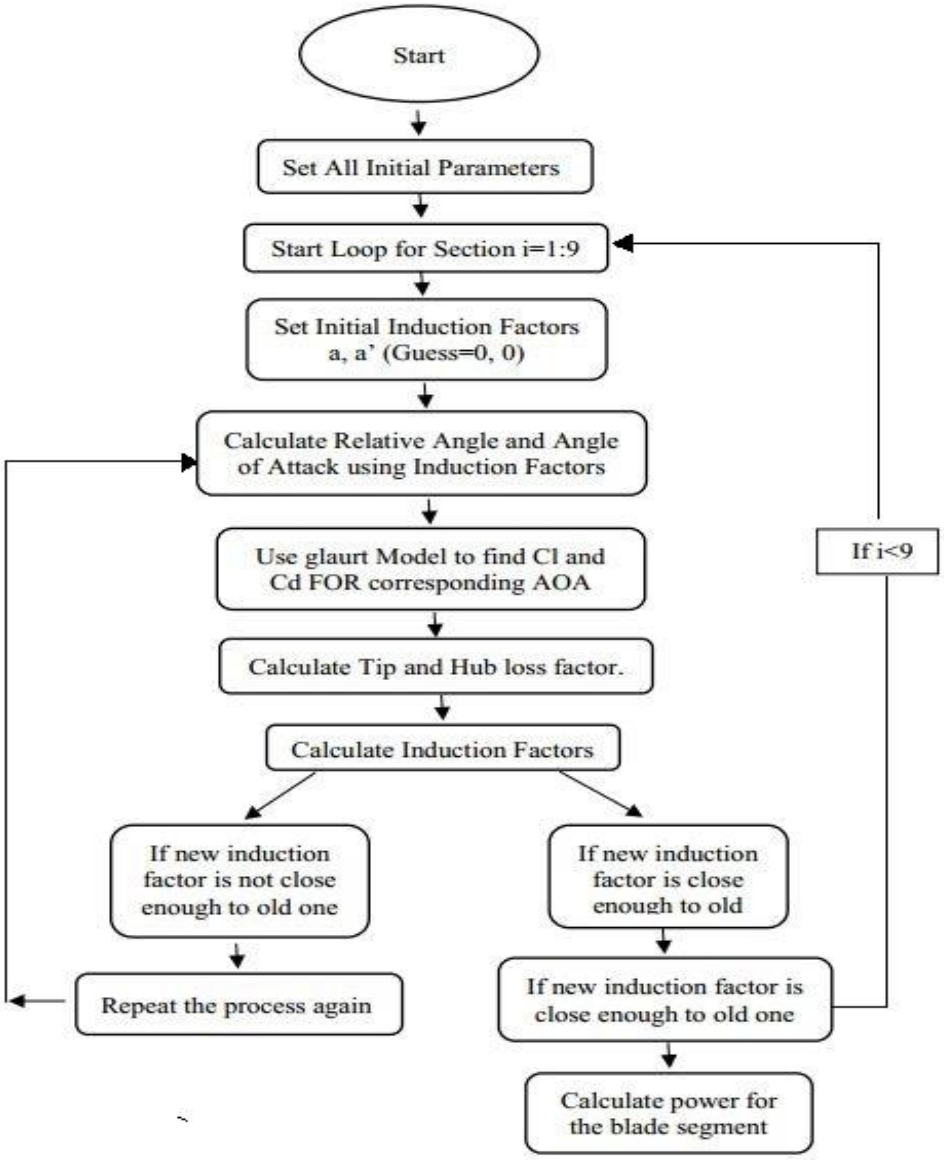

To get the power for each section of the blade first need to calculate Relative speed which can be represented by

$$\boldsymbol{U_{rel} = v * \frac{1-a}{\sin \emptyset}} \tag{3.24}$$

After that tangential force and power for each section can be calculated by the following equations.

$$F_{tangential} = 0.5 * \rho_{air} * U_{rel}^2 * c * c_x \quad (3.25)$$

$$P_{section} = \omega * B * t * F_{tangential} * r \quad (3.26)$$

After computing power for all sections of the blade, the values were added to get whole power for the whole blade. Following equations are used to calculate maximum power, efficiency, and coefficient of performance.

$$P_{Total} = \int_0^n P_{section} dx \quad (3.27)$$

$$P_{max} = \frac{16}{27} * 0.5 * \rho_{air} * v^3 * A \quad (3.28)$$

$$E(\%) = \frac{P_{Total}}{P_{max}} * 100 \quad (3.29)$$

$$C_p = \frac{P_{total}}{0.5 * \rho_{air} * v^3 * A} \quad (3.30)$$

To get the power for each section of the blade first need to calculate Relative speed which can be represented by

$$U_{rel} = v * \frac{1-a}{\sin \emptyset} \quad (3.31)$$

The following equations can calculate that tangential force and power for each section.

$$F_{tangential} = 0.5 * \rho_{air} * U_{rel}^2 * c * c_x \quad (3.32)$$

$$P_{section} = \omega * B * t * F_{tangential} * r \quad (3.33)$$

After computing power for all sections of the blade, values were added to get whole power for the whole blade. Following equations are used to calculate maximum power, efficiency, and coefficient of performance.

$$P_{Total} = \int_0^n P_{section} dx \quad (3.34)$$

$$P_{max} = \frac{16}{27} * 0.5 * \rho_{air} * v^3 * A \quad (3.35)$$

$$E(\%) = \frac{P_{Total}}{P_{max}} * 100 \quad (3.36)$$

$$C_p = \frac{P_{total}}{0.5 * \rho_{air} * v^3 * A} \quad (3.37)$$

3.3 Mixed Airfoil Wind Turbine Blade Design

In a real scenario, due to the rotational speed, different sections of wind turbine blade face different stall conditions. The single airfoil has particular stall condition according to its aerodynamic design. Therefore to regulate the stall condition along the blade span mixed airfoil blade concept was introduced. This work focused on small scale, and in the meantime, the targeted wind speed was supposed to be low. Concentration goes to select airfoils for low Reynold number range. The S series airfoils, which are specialized for wind turbine blade and suitable for low Reynolds number. According to the suggestion given by NREL, three different parts of the wind turbine blade were designed by three different airfoils from S series. In most cases, wind turbine blades include a circular segment to attach to the hub. Then a smooth and gradual transition tapered section is located from the root to first airfoil cross-section. In general, the root side airfoil is the thickest airfoil. Then the thickness ratio gets smaller as it approaches the tip. As S823 is one of the thickest S series airfoils, it was selected for root section of the blade (Somers D. M., 2005). Then, relatively less thick S833 airfoil has been chosen for the middle part, and finally, the S822 Airfoil has been assigned for the tip of the blade.

Table 3**:** Initial design consideration of investigated wind turbine

PARAMETERS	**VALUES**
Expected Power	10kW
Number of blades	3
Rotor radius	5.5 m
Design wind speed	7 m/s
Design Tip Speed Ratio	6
Air density	1.225 kg/m^3
Design Reynold Number	230000

The design parameters stated above table are determined by the same procedure described in section 3.2. All procedures are the same as single airfoil blade design. The only difference here is three mixed airfoil modifications. However, three NREL S series airfoils were tested by Xfoil at designed wind speed. Figure 25 shows the selection criteria of the angle of attack with respect to the ratio of coefficient of lift and drag.

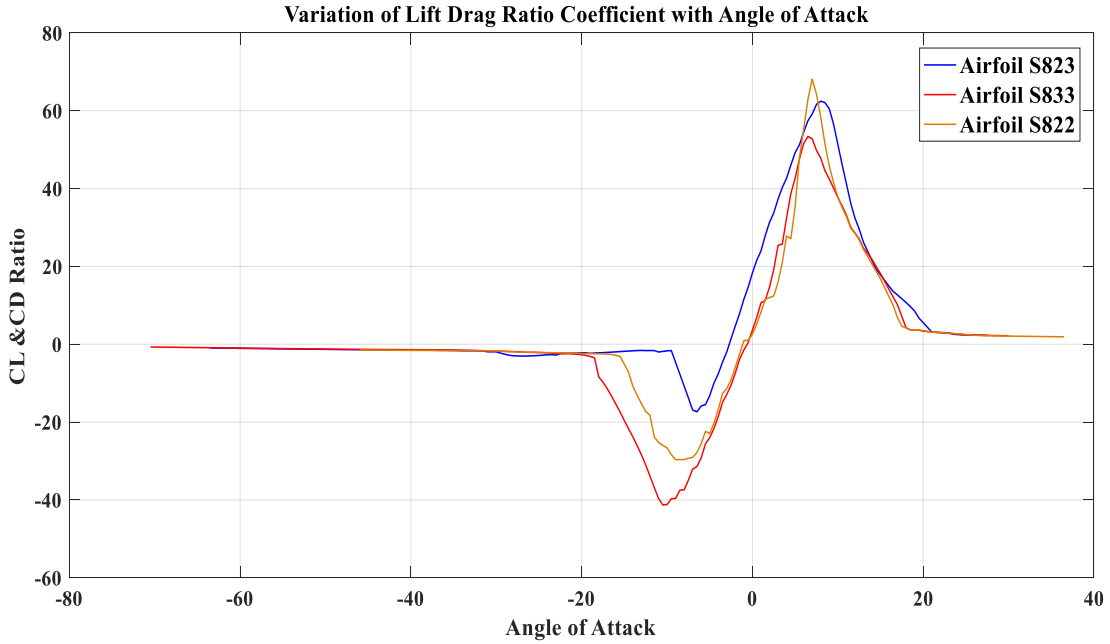

Figure 25: Variation of Coefficient Lift Drag ratio with AOA

From figure 25, it is showed that at the angle of attack 6^0, airfoil S833 has a maximum ratio of Coefficient of lift and drag. At another case for airfoil S822, the coefficient of lift dominates the coefficient of drag in maximum point at AOA 5.5^0. For the third airfoil S823, the maximum ratio happens at AOA 6.5^0. Considering all values, the optimum angle of attack for whole design blade is selected as 6^0. After that, the blade geometry for mixed airfoil turbine blade is considered based on the equations 3.7 &3.8.

Table 4: chord length and twist angles at different sections of designed blade

Relative Radius	Chord Length (m)	Twist Angle (degree)	Airfoil Name
0	HUB	0	HUB
0.15	1.1	28.52	S823
0.25	0.912	15.9625	S823
0.35	0.82	9.6125	S823
0.45	0.704	7.3697	S833
0.55	0.5812	4.9212	S833
0.65	0.4946	3.2004	S833
0.75	0.3846	1.427	S822
0.85	0.34	0.45	S822
0.95	0.3048	-0.329	S822

The above values of chord lengths and twist angles were fixed at the midpoints of the blade segments. Then, a continuous linear loft operation was done between two midpoints of blade segments, next to each other. However, this theoretical optimum blade chord and twist distribution sometimes are not viable for manufacturing. Because the theoretically designed structure, there might have some complexity to manufacture the blade. For this reason, linearization of chord and twist distribution is done by several methods. However, linearization should be done in such a way that the total performance of the wind turbine will remain closer to optimum designed blade performance. Due to simplify the study, this work avoided the linearization of the blade segments parameters. However, a full wind turbine blade solid works model is made according to the dimensions obtained from Table 4. Figure 26 shows the blade model.

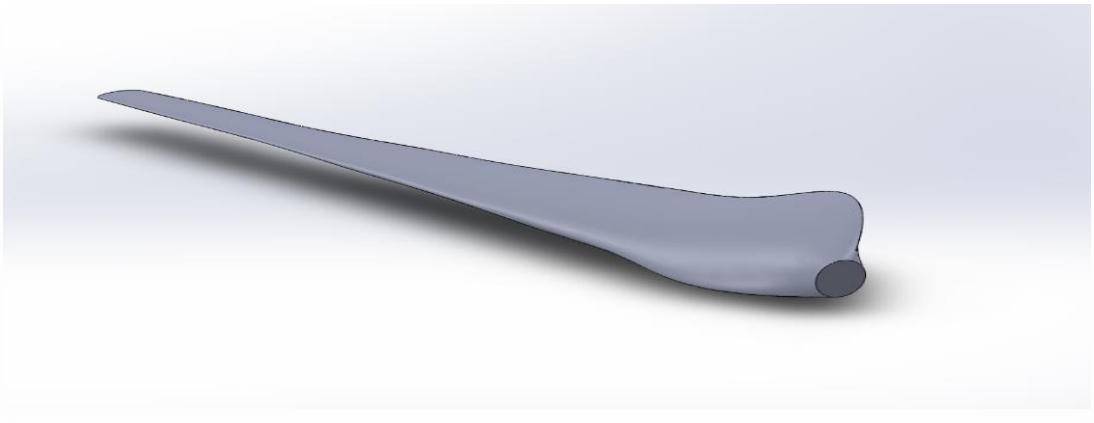

Figure 26: Proposed designed wind turbine blade

3.3 Performance Analysis of Mixed Airfoil Wind Turbine

The entire blade was divided into 40 small elements for BEM analysis. The maximum iteration for this study is set at 100. To ensure the accuracy of BEM, several correction models such as new tip loss, new root loss, 3d correction, Reynold drag correction and foil interpolation are also applied in BEM

3.4 Performance Analysis of Mixed Airfoil Blade by CFD

3.4.1 Governing Equation

The CFD analysis is done based on continuity and Navier-Stokes governing equations. In this work k-ω, Shear Stress Transport (SST) turbulence model was executed in Ansys CFX software. The equations are given below

Conservation of mass is defined by

$$\frac{\partial \rho}{\partial t} + \nabla . \rho \overrightarrow{\vartheta_r} = 0 \tag{3.38}$$

Moreover, Conservation of momentum can be represented as

$$\nabla . \left(\rho \overrightarrow{\vartheta_r} \overrightarrow{\vartheta_r}\right) + \rho\left(2\vec{\omega} \times \overrightarrow{\vartheta_r} + \vec{\omega} \times \vec{\omega} \times \vec{r}\right) = -\nabla \rho + \nabla \cdot \overline{\overline{\tau_r}} \tag{3.39}$$

Where $\overrightarrow{\vartheta_r}$ is relative velocity and $\vec{\omega}$ is the angular velocity (Fluent, 2009).

The blade geometry is imported into a computational fluid domain, which is one-third of a complete circular wind section around the blade. The front side and top side of the domain is defined as the air velocity inlet while rear side is defined as pressure outlet. The other two sides are assigned to the periodic boundary condition. The inlet radius of fluid domain is ten times more than the blade radius. For the outlet radius, the ratio is 20 times. The downstream length of a fluid domain is higher than the upstream length which allows observing the generated wake in fluid domain. After that, the mesh is generated for the entire domain and as well as for the blade

geometry. Figure 27 represents the fluid domain after applying all global and local mesh and mesh control.

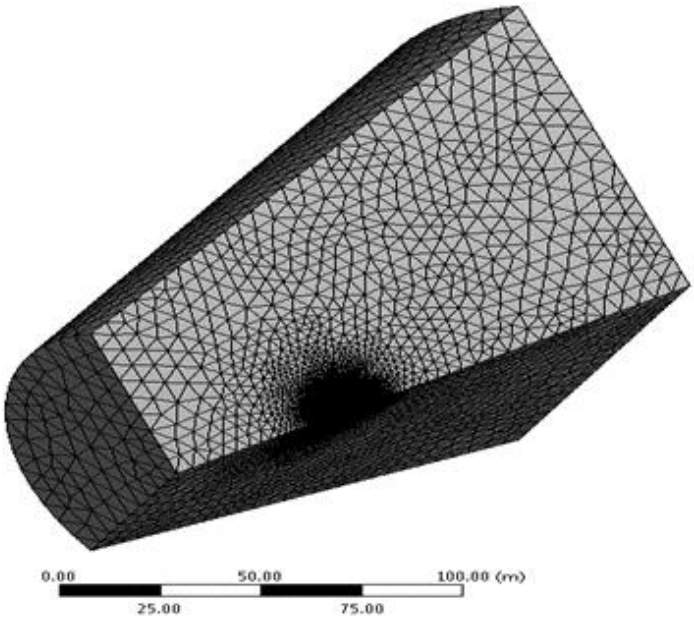

Figure 27: Fluid domain meshing

3.4.2 Computational Domain Meshing

The accuracy of the analysis depends on how the meshing is done. It is good practice to do trial and error for fixing the mesh element size, inflation layer thickness, the sphere of influence radius and so on. For better and uniform meshing the match control is applied between two periodic boundaries conditioned face. This is called local mesh control. One of the key factors of meshing is the variation of element sizing throughout the geometry. Here, the maximum and minimum face element size of the fluid domain are 7.47 m and 0.00747 m respectively. Besides this, the element size of the blade surface was maintained at 0.02 m. An inflation layer was created on the blade surface to give the better resolution of boundary layer flow. The transition ratio was maintained at 0.272 with the growth rate of 1.2. A sphere of influence was also added to fine the mesh around the blade. The sphere radius was 10 m, and element size was 0.4 m (David Hartwanger, 2008) (L.

Wang R. Q., 2016). Figure 28 shows the cross-sectional view of imported blade geometry after applying all global and local mesh control.

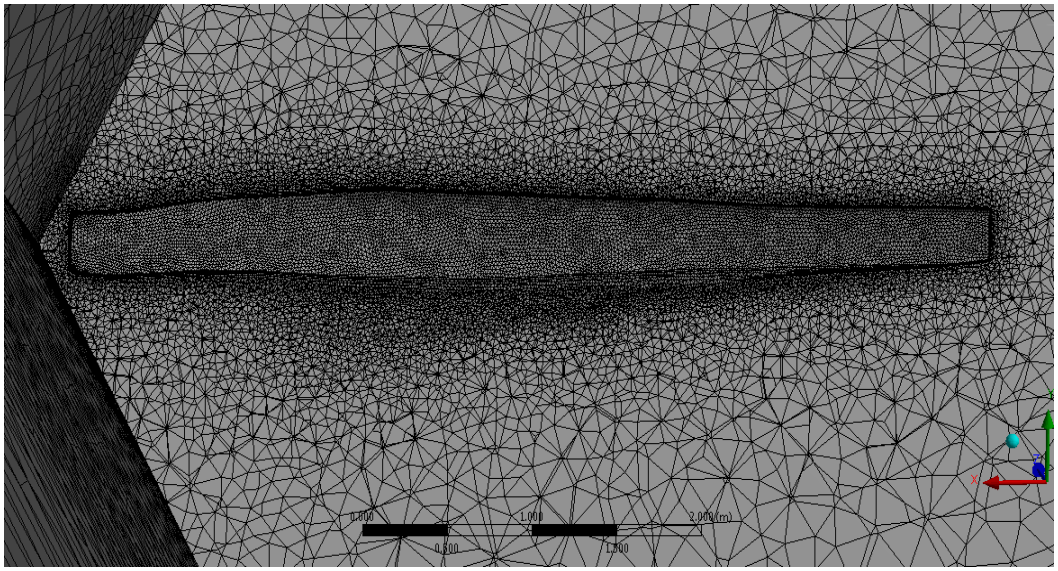

Figure 28: Sectional View of Blade Geometry Meshing

3.4.3 CFD Analysis in Fluent

Finally, the fluent pressure based solver was used to get aerodynamics loading, velocity streamlines, and torque generated by the blade. Here, the fluid flow was considered as turbulent. Among all the turbulence models, k-ω "Shear-Stress-Transport" (SST) model is suitable for this analysis because it can predict the boundary layer separation under the adverse pressure gradient. Menter introduced this model. It is a combination of k-ε and k- ω turbulence model (E.C. Douvi, 2014). The governing equations of k-ω SST model are described below

$$\frac{D\rho k}{Dt} = \tau_{ij}\frac{\partial u_i}{\partial x_j} + \beta^*\rho\omega k + \frac{\partial}{\partial x_j}[(\mu + \sigma_k\mu_t)\frac{\partial k}{\partial x_i}] \tag{3.40}$$

$$\frac{D\rho\omega}{Dt} = \frac{\gamma}{\vartheta_t}\tau_{ij}\frac{\partial u_i}{\partial x_j} - \beta\rho\omega^2 + \frac{\partial}{\partial x_j}[(\mu + \sigma_\omega\mu_t)\frac{\partial\omega}{\partial x_i}] + 2\rho(1 - F_1)\sigma_\omega\frac{1}{\omega}\frac{\partial k}{\partial x_j}\frac{\partial\omega}{\partial x_j} \tag{3.41}$$

Where, $\beta^* = \frac{\varepsilon}{k\omega}$

The turbulence stress tensor can be defined as

$$\tau_{ij} = -\rho\overline{\acute{u}_i\acute{u}_j} = \mu_t\left(\frac{\partial u_i}{\partial x_j} + \frac{\partial u_j}{\partial x_i} - \frac{2}{3}\frac{\partial u_k}{\partial x_k}\delta_{ij}\right) - \frac{2}{3}\rho k\delta_{ij} \tag{3.42}$$

The turbulence viscosity represented by

$$v_t = \frac{a_1 k}{mx(a_1\omega, \Omega F_2)} \tag{3.43}$$

Where Ω absolute value of vorticity, the value of is a_1 is 0.31

The function F_2 is defined by

$$F_2 = tanh\left\{\left[max\left(\frac{2\sqrt{k}}{0.09\omega y}, \frac{500\vartheta}{y^2\omega}\right)\right]\right\}^2 \tag{3.44}$$

Here, y denotes the distance to nearest surface

From the k-ε and k- ω turbulence model, the coefficients β, γ, σ_k and σ_ω can be represented as

$$\beta = F_1\beta_1 + (1 - F_1)\beta_2 \tag{3.45}$$

$$\gamma = F_1\gamma_1 + (1 - F_1)\gamma_2 \tag{3.46}$$

$$\sigma = F_1\sigma_1 + (1 - F_1)\sigma_{k2} \tag{3.47}$$

$$\sigma_\omega = F_1\sigma_{\omega 1} + (1 - F_1)\sigma_{\omega 2} \tag{3.48}$$

$$F_1 = tanh\left\{\left[min\left[max\left(\frac{\sqrt{k}}{0.09\omega y}, \frac{500\vartheta}{y^2\omega}\right), \frac{4\rho\sigma_{\omega 2}k}{CD_{k\omega}y^2}\right]\right]^4\right\} \tag{3.49}$$

Moreover, the coefficient $CD_{k\omega}$ is

$$CD_{k\omega} = \max(2\rho_{\omega 2}\frac{1}{\omega}\frac{\partial k}{\partial x_j}\frac{\partial \omega}{\partial x_j}, 10^{-20}) \tag{3.50}$$

However, to observe the rotational of the blade the standard moving reference frame is used.

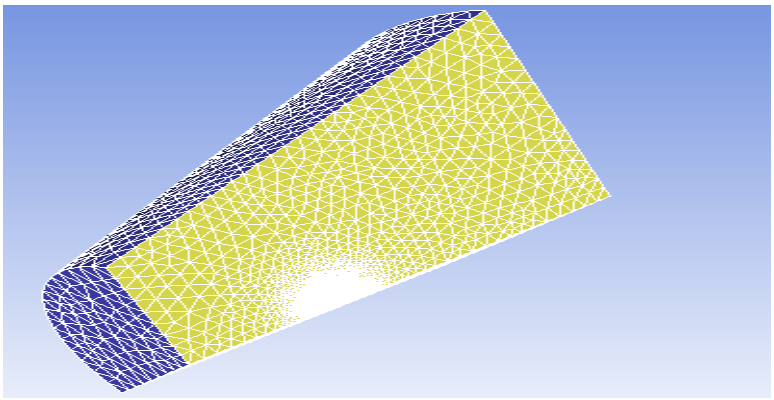

Figure 29: Computational fluid domain in Fluent

This model allows generating a steady state problem on the moving reference. Along with all standard air parameters and operating conditions, the air velocity is applied to the inlet and the top

surface of the fluid domain because air flows not only from the horizontal direction but also from all direction

3.5 Design of Vortex Bladeless Wind Generator

The vortex wind generator was designed by a hollow, conical shaped bluff body which can be placed vertically on the ground. When the air passes over this bluff body, the body experienced vortex induced vibration due to the vortex shedding fluid phenomena. Then, the vibration energy of the body can be converted to electrical energy. Before going to detailed design of the vortex generator, it is needed to clarify the theories behind the working principle. However, the first term is vorticity. The reason behind the vorticity generation is closely related to the fluid dynamics. When fluid flows over a rigid body, a boundary layer is generated at the surface of the body. Due to the shear viscosity of the fluid, shear stress at boundary layer results in the rotational motion at the separation region of the boundary layer and rigid body. This rotational motion of the fluid is defined as vortices. The vortices possess high energy potentiality. It is stated that for a certain Reynolds Number the vortices interact with another which causes instability and turbulence and results into vortex shedding (Wu Jie-Zhi, 2007). Vortex shedding depends on the viscosity and Reynold number of the fluid. In higher Reynold, number inertial forces dominate the viscous forces which cause turbulence. On the other hand in low Reynold number viscous forces is higher than inertial forces which make the flow laminar. There is a certain range of Reynolds number when the disturbance of fluid flow over a bluff body will cause a vortex to be shed. Vortex Shedding can induce high vibration on flexible structures at a certain Frequency. This frequency is a function of Strouhal number which depends on fluid stream velocity and structure diameter. The Strouhl number can be defined as

$$St = \frac{fD}{U} \tag{3.51}$$

Where f is the frequency of vortex shedding, D is characteristics length or diameter of the bluff body, and U is fluid stream velocity (Gabbai, 2005). At higher Reynold Number vortex shedding varies over a narrow band of frequencies and amplitudes. For this reason, strong oscillation of flow is created which leads the formation of Von Karman Vortex effects (Green, 1995). Graebel and at el stated that when a fluid flows over a blunt body, vortices are created and shed in alternating fashion on the top and bottom of the body. This phenomenon will initially be symmetrical but will eventually turn into the classical alternating pattern (Graebel, 2007). Moreover, the repeated, alternating shedding of vortices creates a force that is normal to the general direction of the flow over the body. This load will alternate, corresponding to the side each vortex is shed from. When the load varies in a harmonic manner which causes vibration into the bluff body. The vibration becomes more significant when resonance occurs that means when the frequency of vortex shedding is same as the natural frequency. This resulted in vibration called vortex induced vibrations. The resonance velocity of vortex induced vibration can be defined as

$$V_r = \frac{Nb}{St} \tag{3.52}$$

Where N is natural frequency of body, b is reference crosswind width, and St is Straouhl number (Chen, 2014). The main concern of vortex bladeless wind generator is to utilize vibration energy created by vortex shedding. The bluff body structure is vital factor to get appropriate frequency and energy from vibration. Different types of bluff bodies such as a cylinder, sphere, and conical are available. Among all the bluff bodies the conical shape is suitable for the vortex wind generator. Because in a conical shape, the diameter increases from lower to higher which increases the oscillation of the whole body. The preliminary proposed vortex bladeless wind generator structure

is a conical hollow shape which is supported by cylindrical pipe on the ground. Figure 31 shows the primary model of a vortex bladeless wind generator.

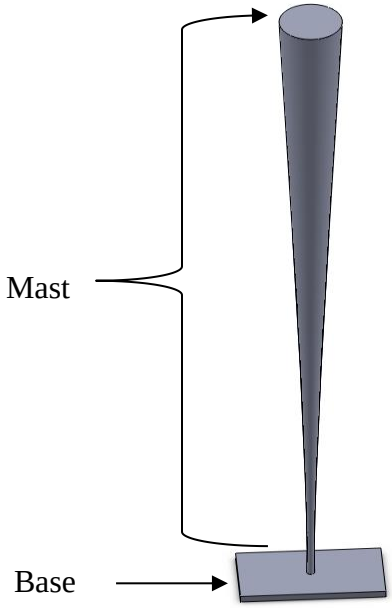

Figure 30: Vortex Bladeless Wind Generator Model

Vortex bladeless wind generators can be placed vertically on the ground. Different parts of the vortex wind generator are mentioned in figure 30. The cross-section of the conical body is a circle. The main parts are Must, stand, and base. The air flows normal to the vertical position of the vortex wind generator. Therefore the whole structure faces von Karman effect due to the air flow. As the entire structure is submerged in the air stream, the von Karman effect varies with the diameter from the top to bottom of the mast. To simplify the analysis of von Karman effect the whole mast is divided into a bunch of small discs with different diameters throughout the cross-section as shown in figure 31. To determine the appropriate diameter of Mast from top to bottom, it is needed to analyze the air flow over the discs of different diameters. In von Karman effect, oscillation mainly depends on the Reynold number, air velocity, diameter of the submerged object or disc, and as well as the air flow direction. However, in von Karman effect vortex shedding is created at

sinusoidal manner. The force which leads the vibration of vortex structure is lift force due to air passing on it.The lift force can be defined as.

$$F_l = \frac{1}{2}\rho U^2 D C_L \sin(\omega_s t - \varphi) \tag{3.53}$$

Where ρ is air density, U is air velocity, D is the diameter of the crossection of Mast, Cl is lift coefficient, $\omega_s$is vortex shedding frequency and t is time . When the whole conical structure is divided into small element, indidivually the elements can be treated a small cylinder with neglible length like circular disc. Vortex wind turbine with differen dimensions is tested for von Karman effect. Figure 31 describes the dimensions of vortex wind turbine model.

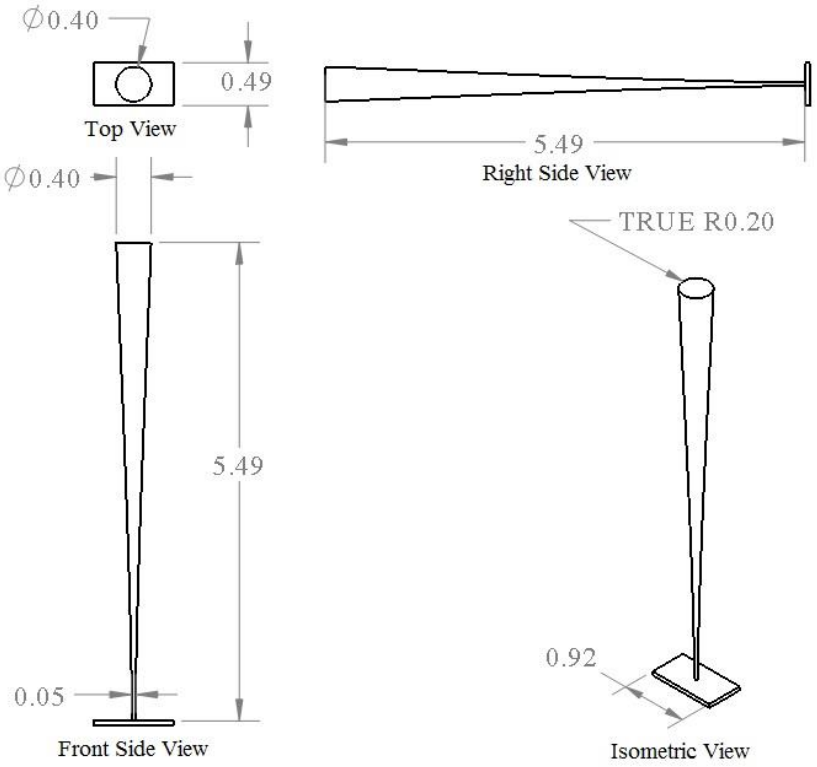

Figure 31: Detailed dimension of Vortex Bladeless Wind Generator

After the von Karman analysis and dimension fixation, the whole vortex structure is placed into a fluid domain for Fluid-Structure Interaction analysis. Ansys fluent and Ansys structure tool is used for the simulation process. Figure 32 shows the cross-section of the meshed fluid domain with vortex wind turbine.

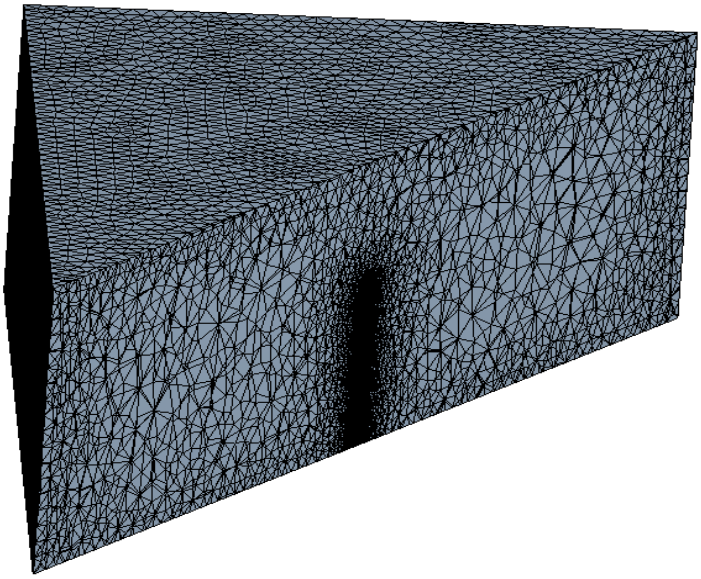

Figure 32: Fluid domain with vortex wind turbine and mesh analysis

The energy absorption by vortex wind generator depends on the displacement of the mast. Therefore fluid-structure analysis (FSI) is applied to determine the displacement of mast displacement.

CHAPTER 4

RESULTS

4.1 Performance Analysis of Single Airfoil Wind Turbine Blade

The whole study is divided into three main sections. In the first section, a small-scale horizontal axis wind turbine blade is designed. The blade is made by the single airfoil. The optimum chord lengths and relative angles are designed for different locations along the radial distance with the objective of maximizing the lift to drag ratio as well as blade performance. In this work, the pitch angle is fixed. That is why the twisting of the blade is done according to the optimum angles of attack and relative angles. The coefficient of performance, power, and torque was calculated by BEM method. At the preliminary stage of BEM, Glauert wake correction model was applied along with the Prandtl tip loss correction loss. Figure 33 shows the variation of coefficient of performance for different tip speed ratio.

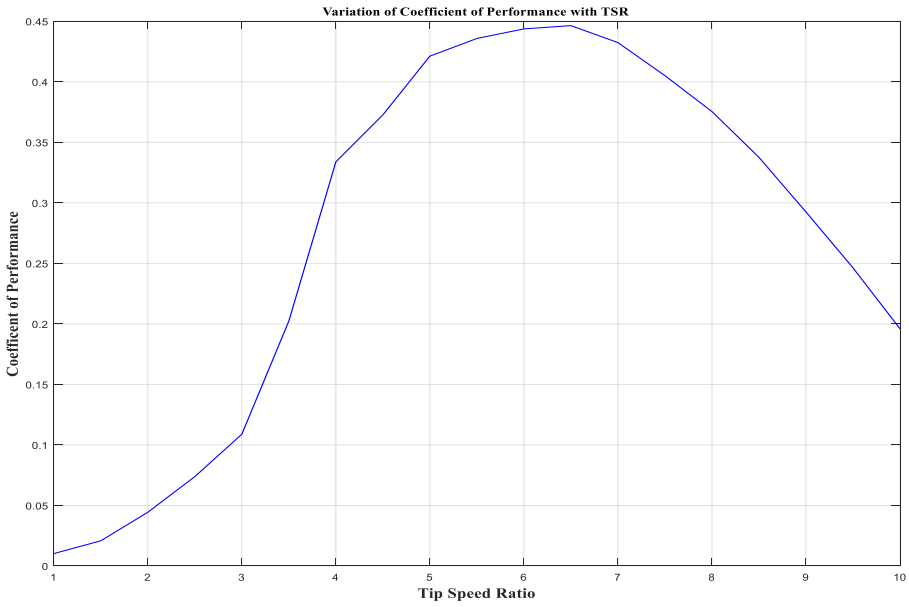

Figure 33: Variation of Coefficient of Performance with Tip Speed Ratio

It is noted that the new tip loss correction, New Root loss correction, 3D Correction, and Reynold Drag Correction is also applied to get accurate results of performance analysis. From the figure 34, it can be showed that the nature of the curve of performance is similar to the traditional wind turbine. Here the analysis is done between the tip speed ratios one to ten which is the range for a horizontal axis wind turbine. From the performance curve at figure 34, it is showed that the highest coefficient of performance is 0.446 at Tip speed ratio 6.5. Moreover, in this case, the efficiency and power outputs are and 8.12 kW respectively. From the figure, it is noticed that the best tip speed range for this work is five to seven. Here it is noticeable that design Tip Speed Ratio was considered as 6. Obviously the best performance is achieved at Tip Speed Ratio around 6. Therefore tip speed ratio is a function of wind velocity; it can be said that the power output does not deteriorate even the wind velocity fluctuates at a certain range. BEM is done element-wise. In every element, iterations are done until the convergence of induction factors. Figure 34 shows the angle of attack in different blade position.

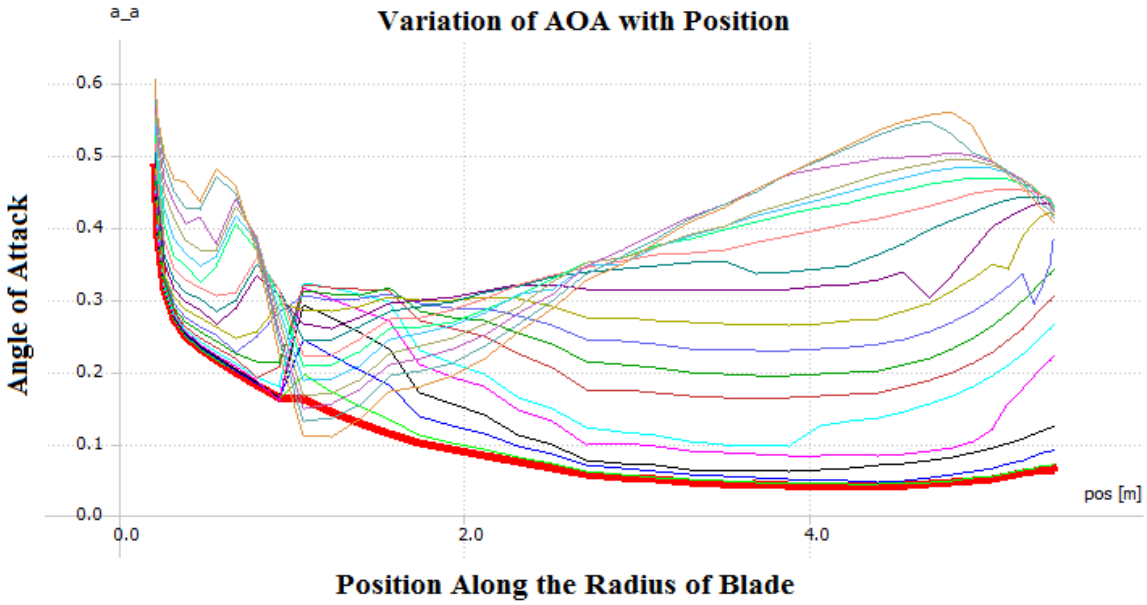

Figure 34: Variation of Angle of Attack along the radius of the blade

From the figure 34, it is concluded that after 1 m from the root a certain drop of attack angles in every iteration. This is due to sudden change of twist angle within a small distance from the root. The first twist angle is very high compared to other twist angles of the blade. After 2 m the angles of attack change uniformly according to twist angles.

4.2 Performance Analysis of Mixed Airfoil Wind Turbine Blade

In the second part of the study, a horizontal axis wind turbine blade with mixed airfoil was designed for performance improvement. The airfoils are S823, S833, and S822. The performance analysis of mixed airfoil blade was done with same parameters and environment as the single airfoil blade. The turbine operating conditions also set as fixed pitch and variable speed. Figure 36 shows the Comparison of Coefficient of Performance between Single Airfoil Blade and Mixed Airfoil Blade

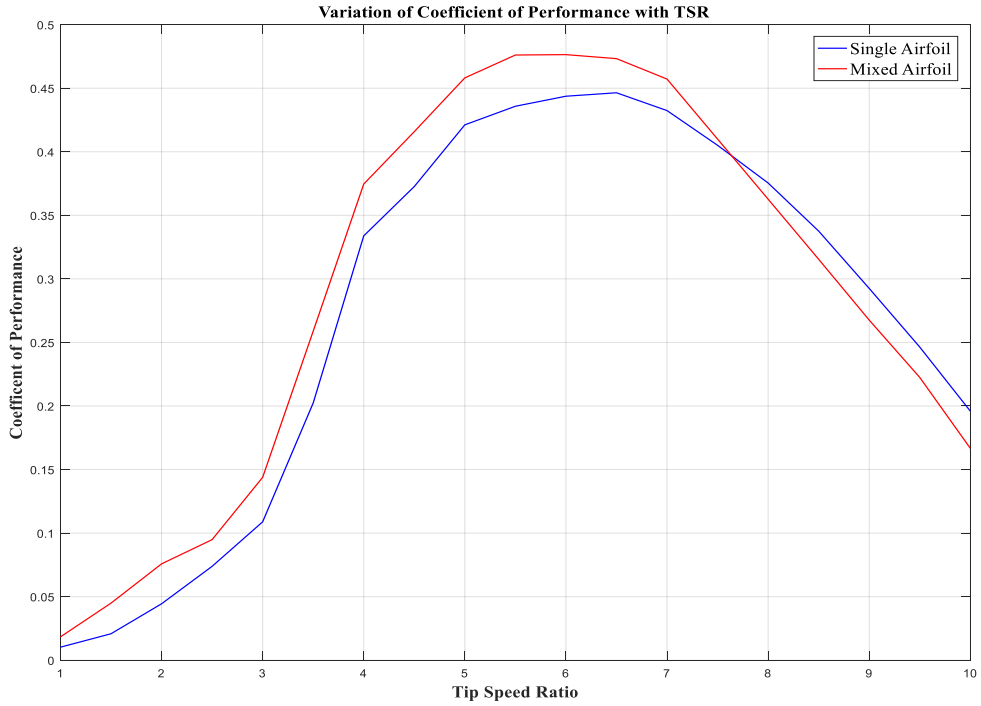

Figure 35: Comparison of Coefficient of Performance between Single Airfoil Blade and Mixed airfoil blade

It is clear that the modification of blade by adding different airfoils leads the increase of performance. From the figure, it is noticeable that the maximum coefficient of performance of mixed airfoil wind turbine is 0.475 where maximum value for single airfoil blade is 0.446. At mixed airfoil blade, the maximum power was reached at Tip speed ratio 5.5. However, for mixed airfoil blades, the maximum performance stability region is more than the single airfoil blade. In the case of mixed airfoil blade, the coefficient of performance for Tip Speed Ratio up to 7.5 is higher than the single airfoil blade. Whenever Tip Speed Ratio is increased from 7.5, the performance curve uniformly decreased. From this kind of behavior, it can be concluded that the mixed airfoil blade is good for low tip speed ratio comparing with single airfoil blade. The associative parameters with performance were also analyzed Figure 36, 37 and 38 show the comparison of the coefficient of thrust, power, and torque with the Tip Speed Ratio.

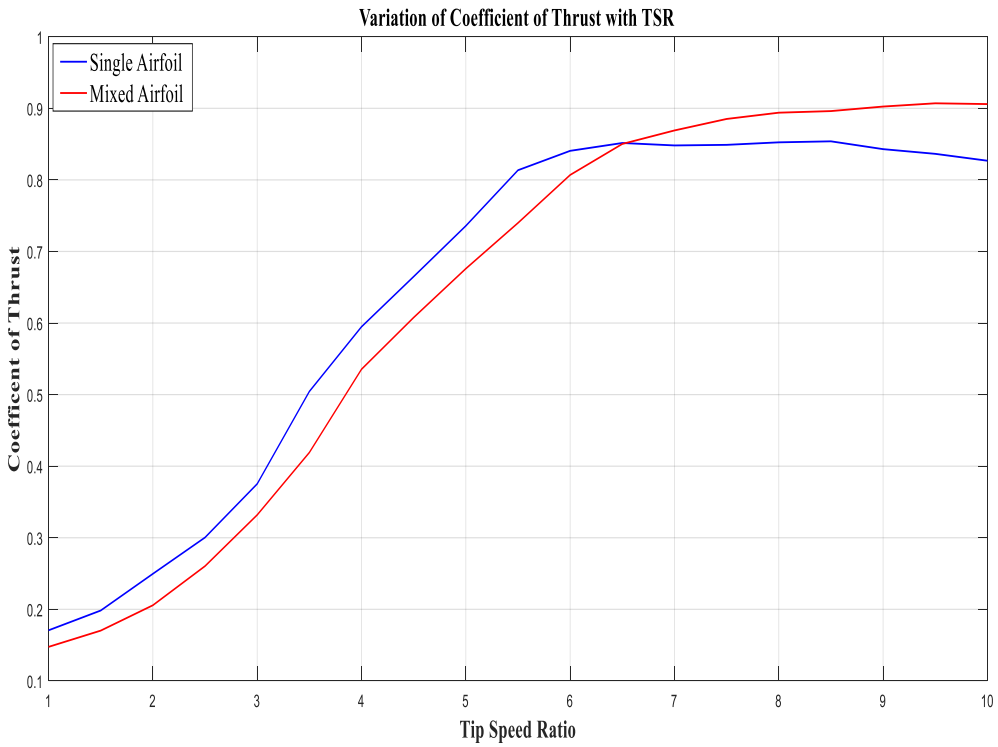

Figure 36: Coefficient of Thrust variation with Tip Speed Ratio and Comparison

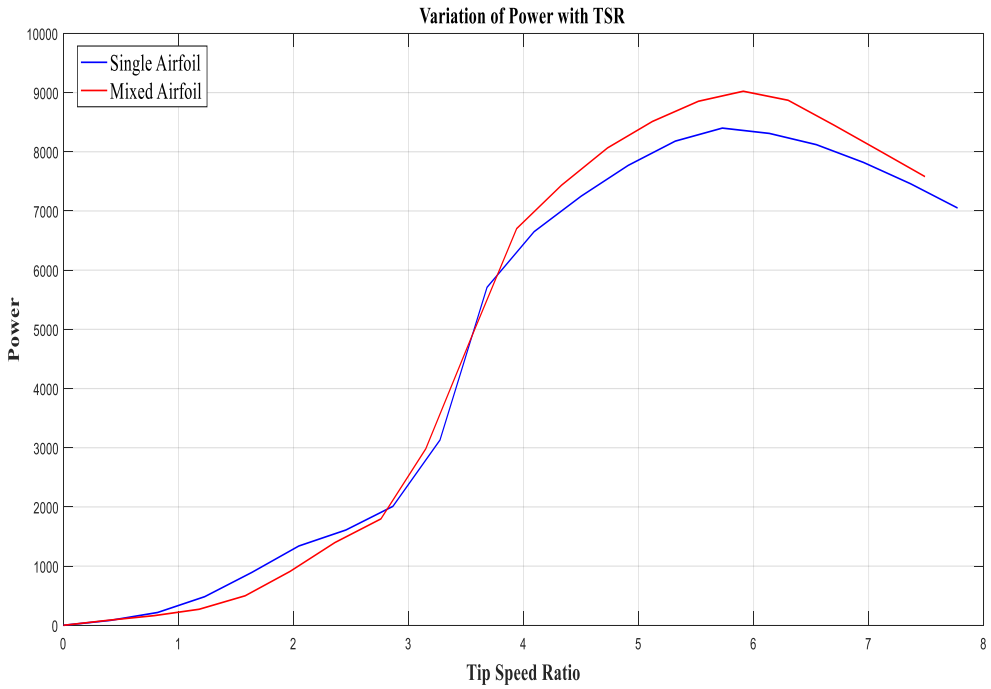

Figure 37: Variation of Coefficient of Thrust with Tip Speed Ratio and Comparison

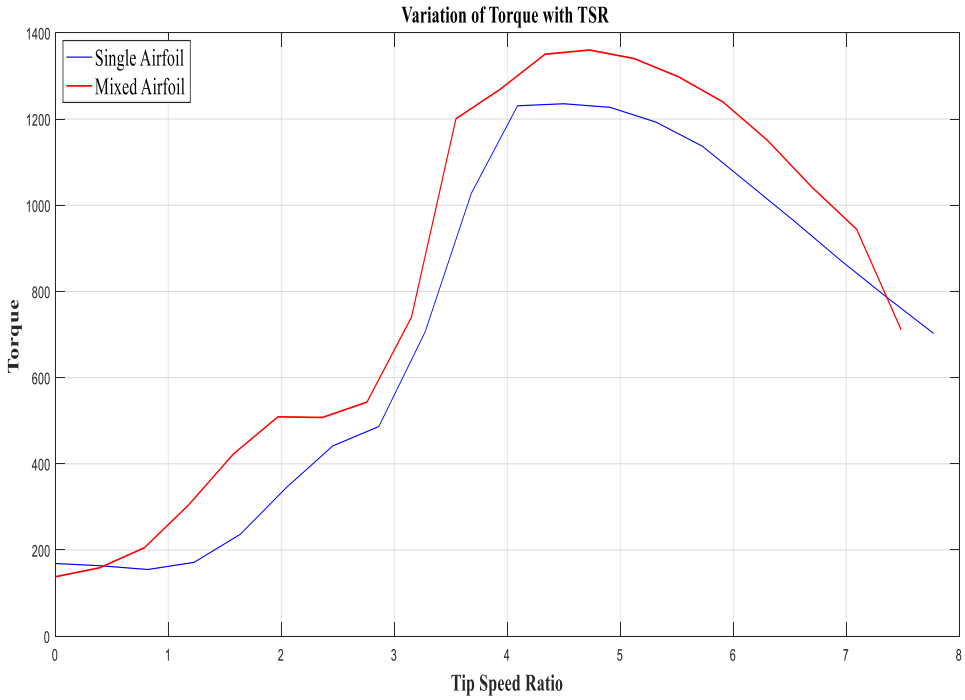

Figure 38: Variation of Coefficient of Torque with Tip Speed Ratio and Comparison

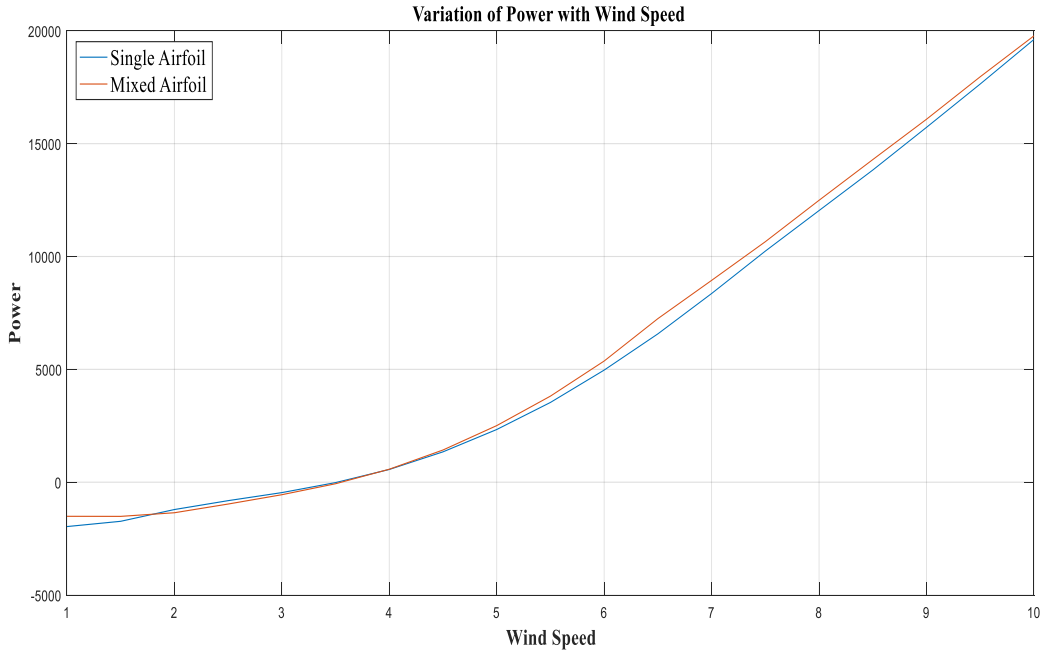

Figure 39: Variation of Power with Wind Speed and Comparison

Figure 36 shows that the thrust coefficient behavior is opposite to the coefficient of lift. The single airfoil blade thrust coefficient is higher than the mixed airfoil blade thrust coefficient at low Tip Speed Ratio range. On the other hand, when TSR reaches 6.5 or more the scenario is opposite. Figure 38 & 39 show the power and torque variation with TSR. As power depends on torque, the both figures show the same pattern. It noted that actual maximum power obtained from mixed airfoil wind turbine is 9 Kw, which is close to the expected value. However, figure 39 represents that power increases proportionally with the wind speed. When the wind speed is lower than 5m/s, the increasing rate of power is slow. However after 5 m/s wind speed, the power increases sharply.

4.3 CFD Analysis Results of Mixed Airfoil Wind Turbine Blade

Compressible Fluid Dynamics analysis is done to investigate the performance of small scale mixed airfoil wind turbine blade. Here k-ω SST turbulence model is used to investigate the air interaction. However, CFD post is used to observe the results of the simulation. Figure 41 shows the axial

velocity of the blade at a tip speed ratio 6. Here, the wind velocity is maintained at 7 m/s. Moreover, rotational velocity is fixed at 7.63 rad/s.

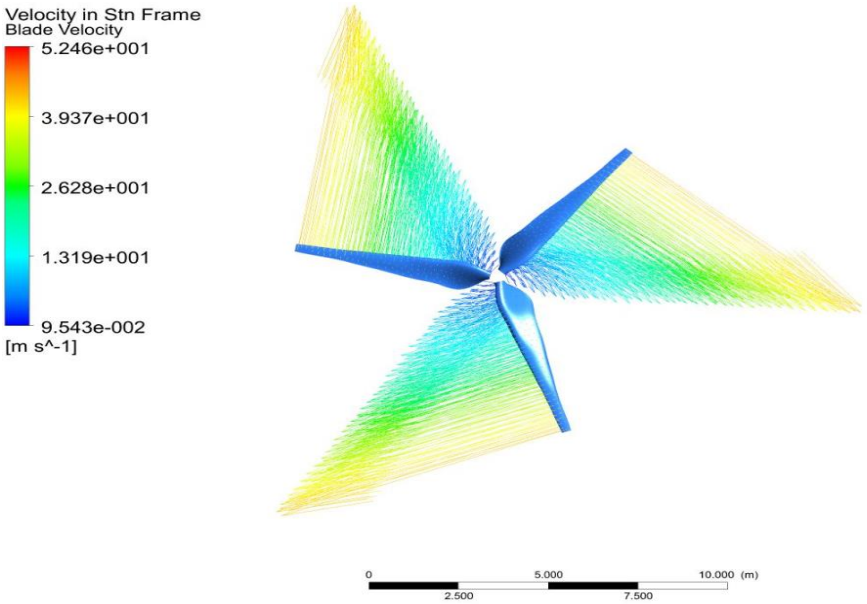

Figure 40: Axial Blade Velocity Distribution

From figure 40, it is visible that the axial velocity of the blade varied throughout the blade length. The blade velocity increases from the blade root to tip. As expected from the conventional wind turbine theory, the velocity at the tip is the highest velocity. Moreover, the axial velocity increases at a uniform pattern. For this reason, wind turbine blade faces outward centrifugal force. Therefore, the axial velocity observation will help in stress analysis of the blade. The air flow through the fluid domain is also observed in CFD-post. There is a small drop in air velocity after passing the turbine blade. The reason behind this is the wake formation by turbine rotor. As compared to all the air streamline of the fluid domain, the wake formation is slight, and that can be on a negligible scale. The less wake formation leads fewer energy losses. The currently designed wind turbine can give better performance in the point of view of wake formation. On the other hand, a sudden increase of air velocity is observed around the tip of the blade. The reason behind this is the blade rotation.

From this observation, the mass momentum criteria of energy conservation phenomena are fulfilled. Figure 41 represents the air flow visualization for designed small wind turbine rotor

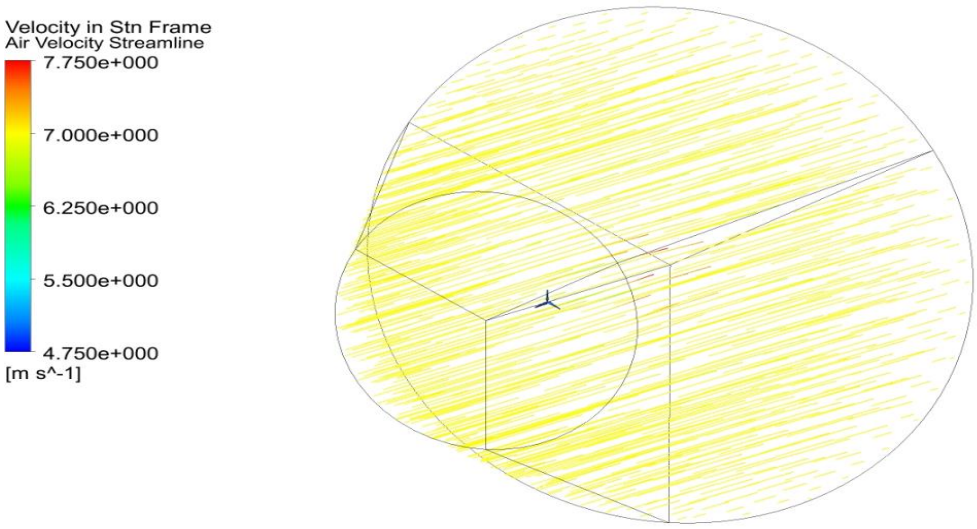

Figure 41: Air Flow Visualization

The pressure distribution on blade spanwise is showed in figure 42. It is noted that there is a clear pressure difference between upward surface and the downward surface of the blade which prevails the wind turbine main aerodynamic principle. The close investigation showed that the pressure difference is higher at tip portion compared to the root part of the wind turbine blade. In other words, there is a low-pressure area at the tip leading edge of the blade. The reason behind this is the three-dimensional rotation effect of the wind turbine blade tip.

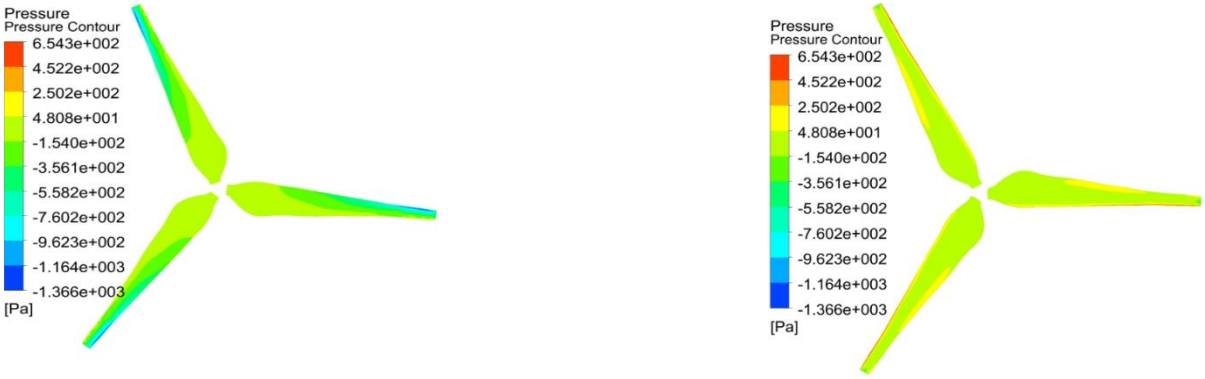

Upward side of Blades Downward side of Blades

Figure 42: Pressure Distribution on blade surfaces

Airflow separation is also observed by CFD post. Figure 44 represent the flow separation by blade at 2.5 m radius in case of three different air velocities.

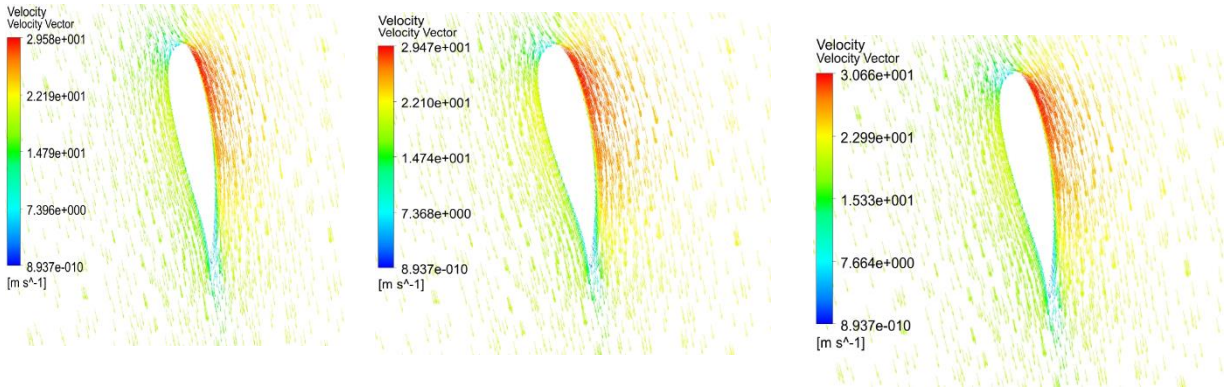

At air velocity 4 m/s At air velocity 6 m/s At air velocity 8 m/s

Figure 43: Air Flow Separation Observation

From figure 43, it is noticed that, the flow separation remains same at all wind velocity range of small scale. From the close observation it is showed that at the top front side of the airfoil wind passes at high velocity comparing with other part of the blade. However there is an opposite relation between wind velocity and pressure distribution during the air flow over the airfoil Pressure distribution at 2.5 m radius for different air velocity is also observed at figure 45.

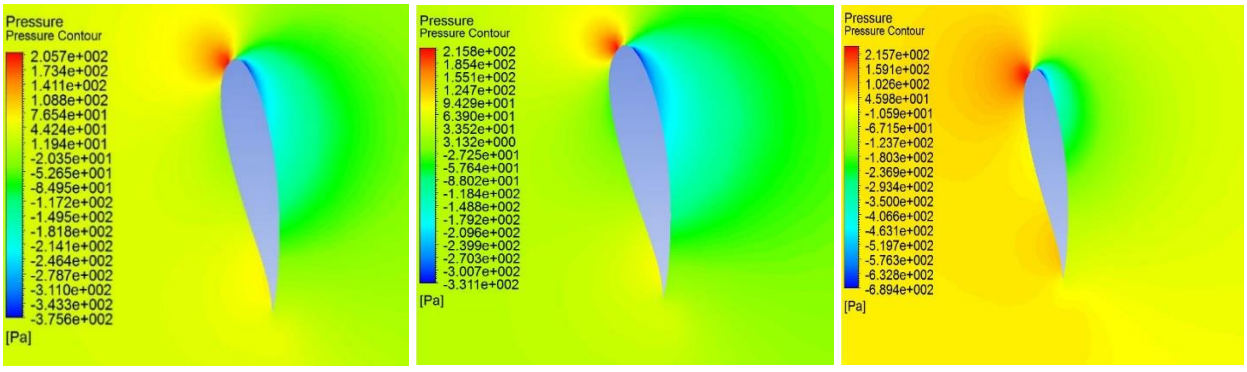

At air velocity 4 m/s At air velocity 6 m/s At air velocity 8 m/s

Figure 44: Pressure Distribution Observation

From figure 43 and 44 it can be concluded that around the blade surface where velocity increases, pressure decreases. This is completely followed the working principle of lift type horizontal axis wind turbine. A span-wise flow separation analysis is also done. Figure 46 shows the velocity vectors along the blade radius.

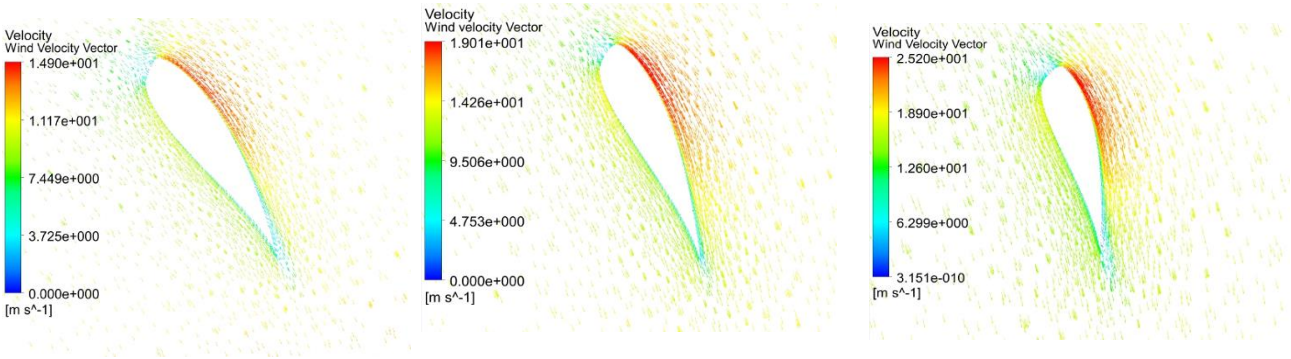

Cross-section at 0.825 m radius Cross-section at 1.375 m radius Cross-section at 1.925 m radius

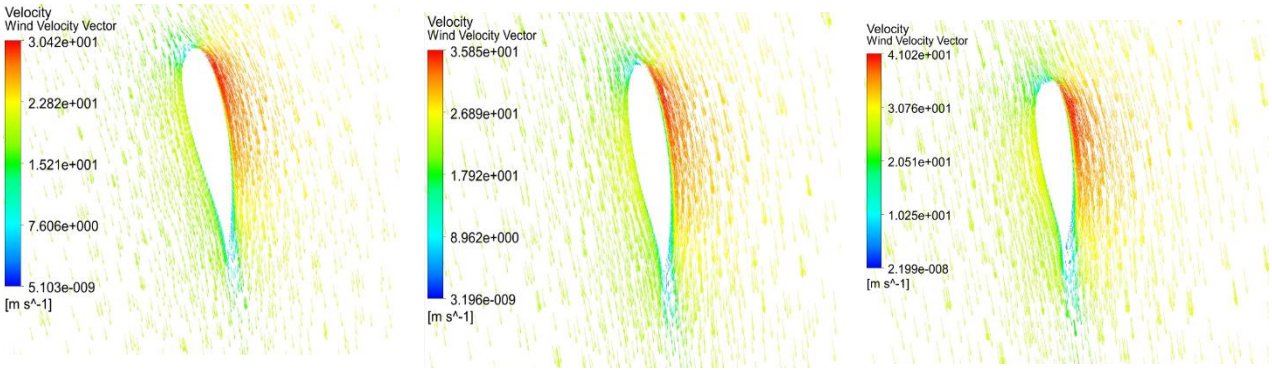

Cross-section at 2.475 m radius Cross-section at 3.025 m radius Cross-section at 3.575 m radius

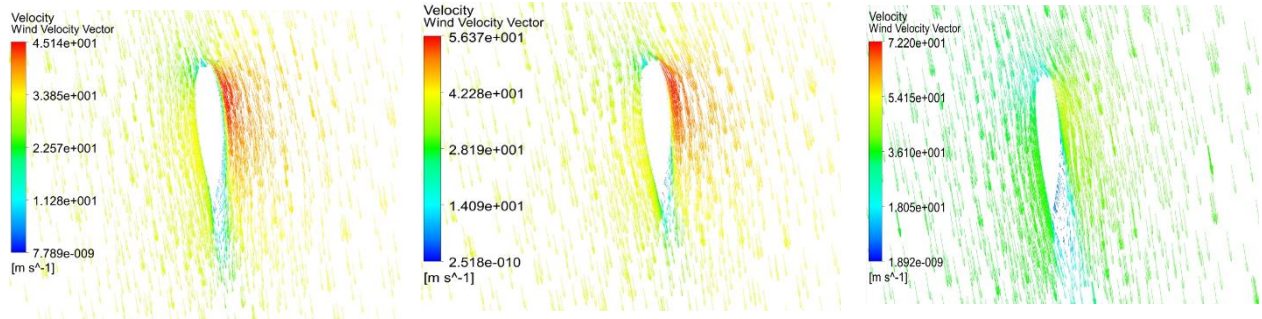

Cross-section at 4.125 m radius Cross-section at 4.675 m radius Cross-section at 5.225 m radius

Figure 45: Flow Separation Observation

From figure 45, it is observed that the flow separation increases from root to tip of the blade. This is happening because at the tip the air slips in the outward direction, so a complex flow pattern is created at blade tip which leads the stall condition of the blade. Pressure distribution along the blade radius is also observed by CFD post. Figure 46 shows the pressure distribution.

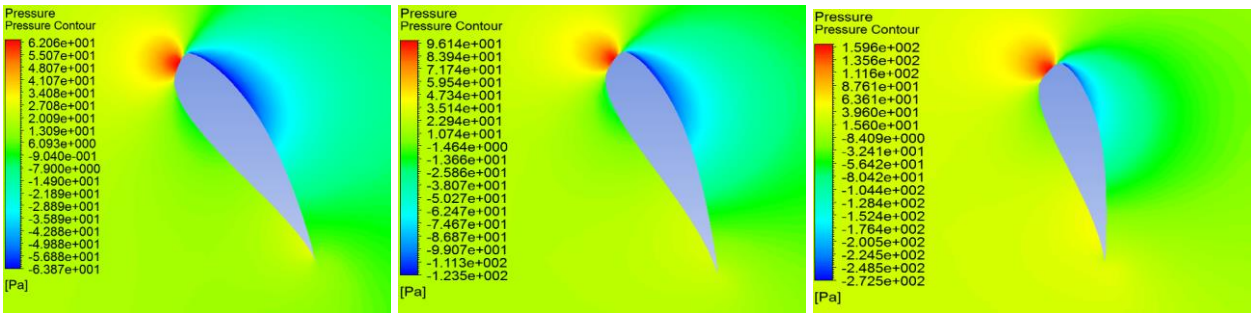

Cross-section at 0.825 m radius Cross-section at 1.375 m radius Cross-section at 1.925 m radius

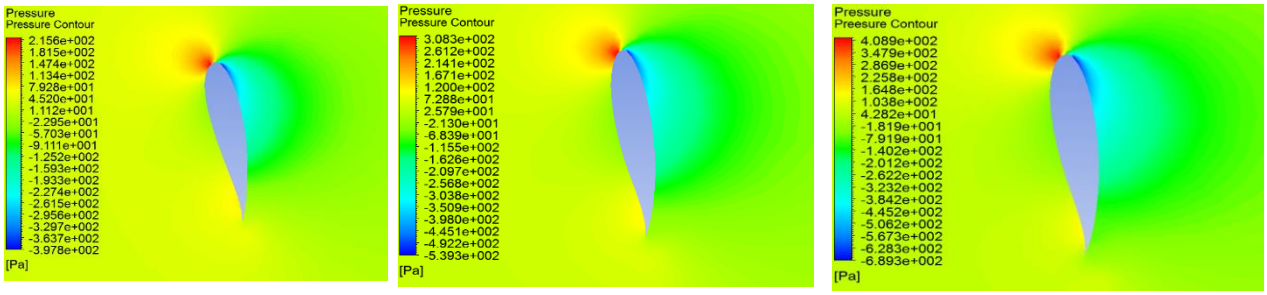

Cross-section at 2.475 m radius Cross-section at 3.025 m radius Cross-section at 3.575 m radius

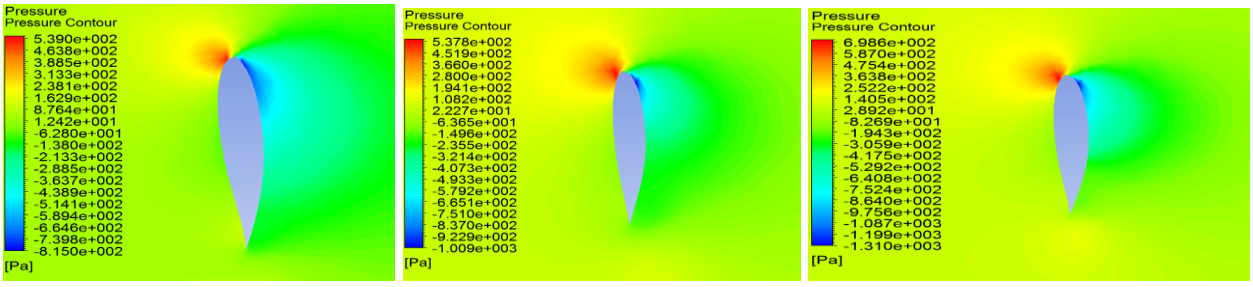

Cross-section at 4.125 m radius Cross-section at 4.675 m radius Cross-section at 5.225 m radius

Figure 46: Pressure Distribution along the Blade Radius

Finally, a comparison between performance results by BEM and CFD method is done. Figure 47 represents the comparison.

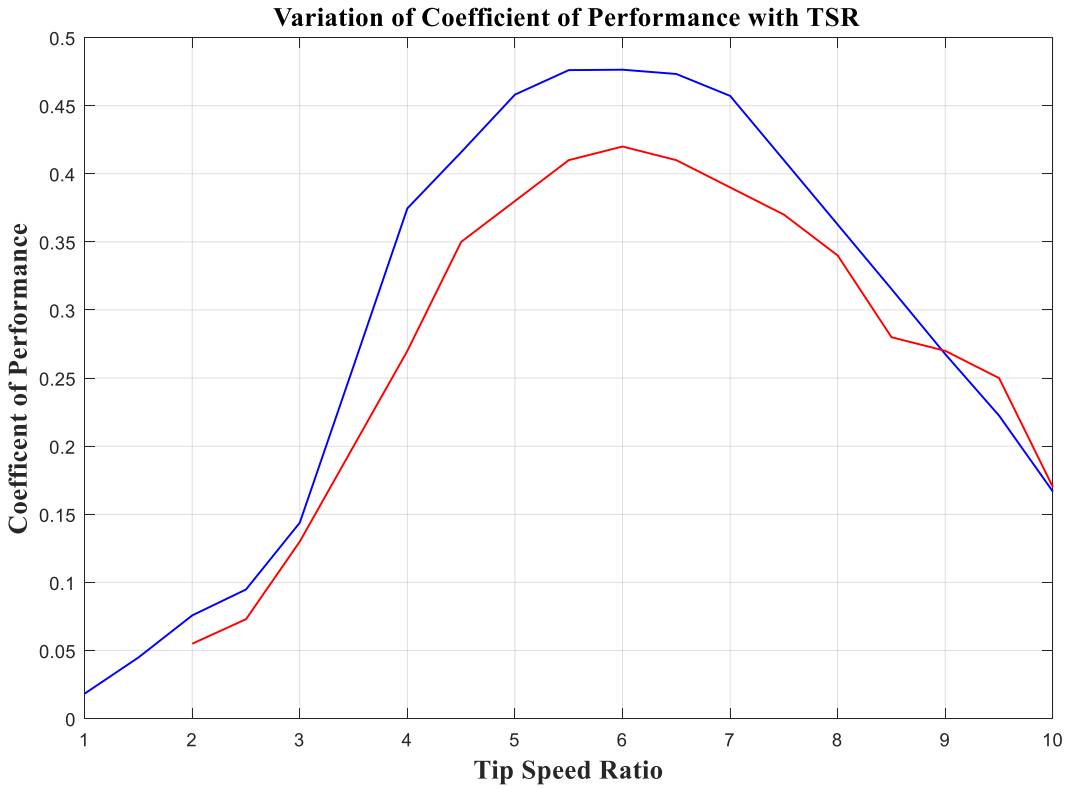

Figure 47. Comparison between BEM and CFD

In current study performance of wind turbine was determined against different Tip Speed Ratio (TSR). From coefficient of performance (COP) vs. Tip Speed Ratio (TSR) curve analysis, it is clear that the performance of wind turbine blade by CFD computation is a little bit less than BEM. The CFD method can calculate more accurately with 3D calculation than BEM. Figure 47 shows that initially at low TSR the rotational speed is very low in both cases. After the TSR 3, the COP increases sharply in BEM, whether in CFD the COP increase gradually with TSR up to 5. After that, in the BEM analysis, the COP is more stable than in the CFD within the TSR range 5 to 7. For both cases, the maximum COP has reached at TSR 6. After that, with the increasing of tip speed ratio, the coefficient of the performance goes down. The reason behind this is the stall condition of the wind turbine which is described by Betz limit of the wind turbine. However, the highest coefficient of performance in BEM is 47% and in CFD method it is 43%. Both of the

values remain within the Betz limit. The difference between both method's results is 4%. One of the reasons for this difference is that, the over prediction of xfoil software for obtaining lift and drag coefficients. Though all kind of correction models are applied in BEM, the CFD results provide more detailed visualization of wind turbine response to get a complete idea about performance. The BEM has the limitation of computation for rotational motion as compared to the CFD. In CFD the predetermined aerodynamic data is not used to predict the performance. Instead of that CFD solver computed governing fluid equations at all direction around the blade. This approach allows the blade to analyze any span wise wind speed as well as the three-dimensional fluid body interaction effects including friction losses. However, the BEM method cannot do this kind of analysis. Finally, it is concluded that BEM can be used for initial estimation and then the wind turbine's design can be optimized with the detailed observation by CFD method.

4.4 Vortex Blade less Wind Turbine Simulation Results

In the third part of this study investigation of the possible extraction of power from wind energy by using a new conceptual vortex bladeless wind generator is done. First the vortex wind turbine design parameters are selected. After that dimensions are determined based on the Von Karman effect analysis by Ansys.

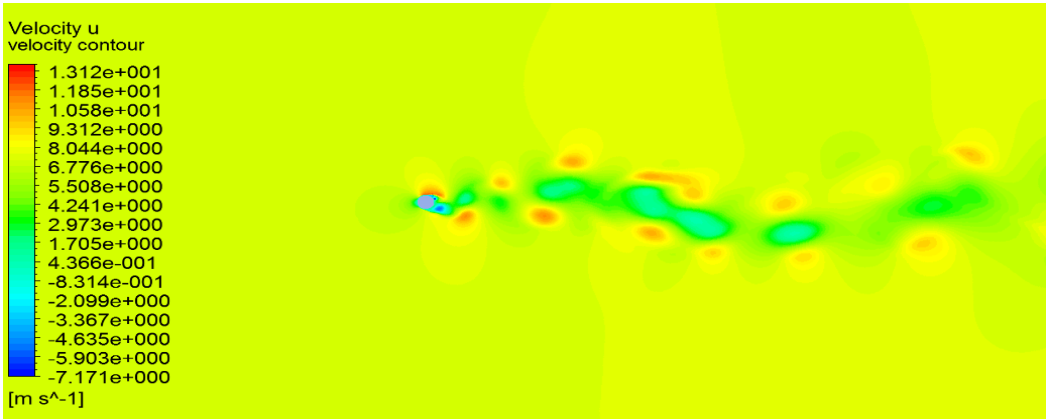

Figure 48: Von Karman effect around the top surface of the designed vortex turbine

Figure 48 shows the Von Karman effect at air passing over the vortex blade. Here it is showed that the air continuously changes the direction of flow after passing the bluff body structure. The Velocity flow field is showed in figure 49.

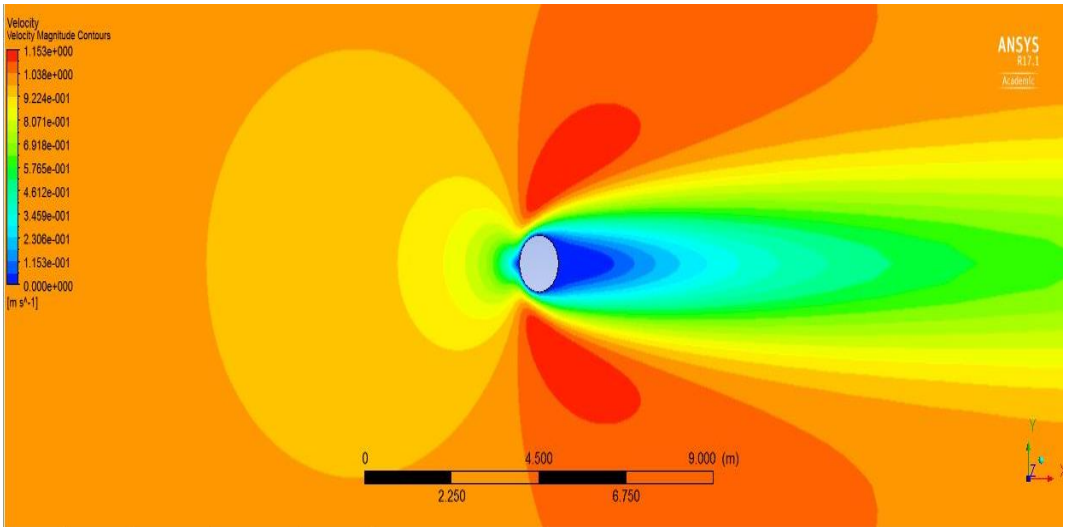

Figure 49: Velocity Contour in air flow field passing over the vortex turbine

It is clear that a certain velocity drop happens at the middle downstream and close position of Mast cross section disc, when air passes over it. On the other hand air velocity increases at both sides of the disc. The consequent pressure distribution is presented in figure 50.

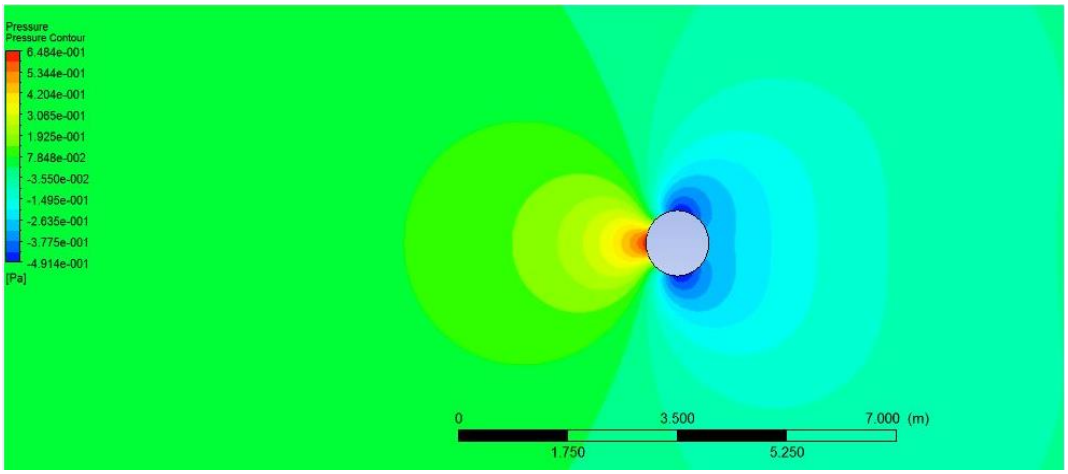

Figure 50: Pressure Contour in air flow field passing over the vortex turbine

The pressure distribution is opposite to the velocity distribution. The lowest pressure is located at two sides of the disc. However, this pressure drop leads further turbulence of air. Moreover, due

to the turbulence, a sinusoidal lift force is created in the flow field. Figure 51 represents the coefficient of lift due to the Von Karman effect on vortex turbine Mast. This lift results vortex induced vibration on the submerged conical Mast.

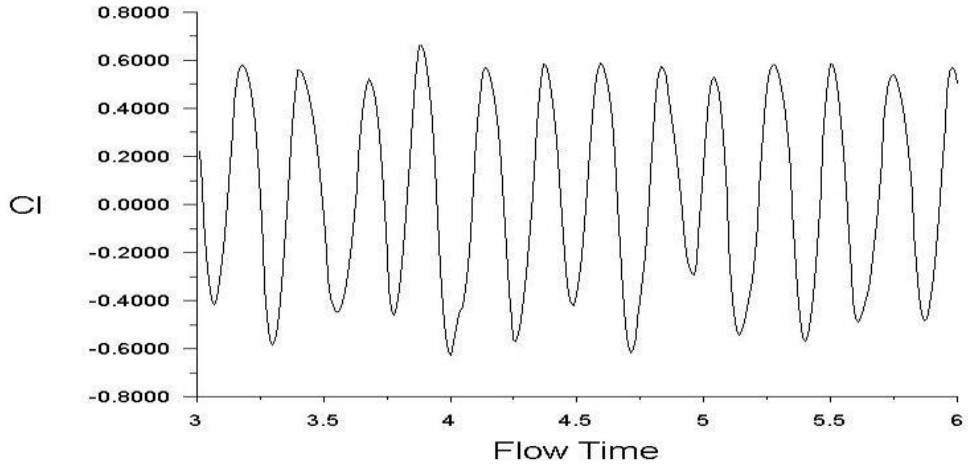

Figure 51: Variation of Coefficient of lift with time

The vortex-induced vibration can show some reactions during the operation. Sometimes, the vortex shedding could become more strong. Sometimes, the wake may become more correlated across the body. In some cases the average drag may increase. The variation of coefficient of drag with the time is given in figure 52.

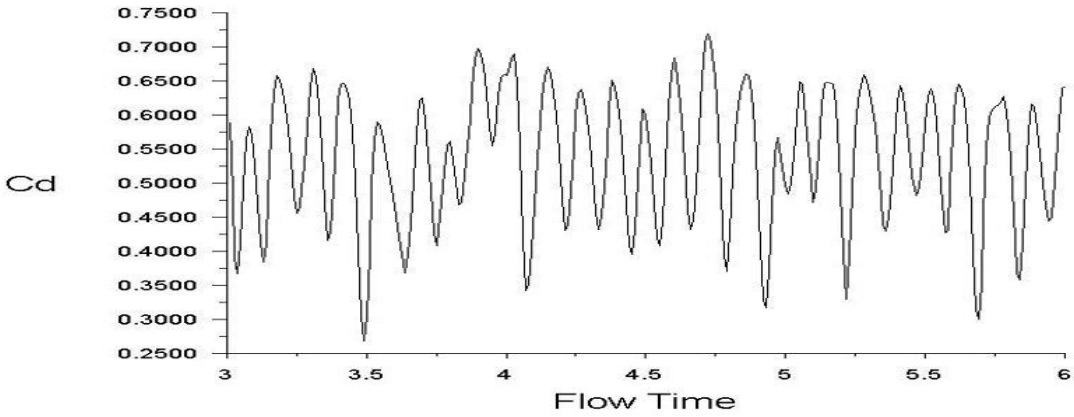

Figure 52: Variation of Coefficient of drag with time

The most significant reaction occurs when the vortex shedding frequency synchronizes with the Mast's vivration frequency. This is called lock-in condition. Due to the adjustment of air flow the vortex shedding frequency approaches to the body's natural frequency. This will apply a significant amount of vibration energy to the body.

CHAPTER 5

CONCLUSION

This thesis presents the research on small wind energy sector which is one of the potential renewable energy sources. With the aim of finding reliable solution for a power source for Nano grid, the research is conducted on small scale wind technologies. However, the research concentrates on design and modification of small scale horizontal axis wind turbine blade. After that performance analysis of designed blade is done by two most reliable methods, BEM and CFD. As an extension of research on small wind energy systems, the potentiality of vortex bladeless wind turbines is also explored. The major findings are described below.

- Instead of using multiple micro wind turbines, a single small scale wind turbine with comparatively larger diameter (still in small scale range) can produce sufficient power for Nano grid.
- In the fixed pitch small scale wind turbine, the compensation made by blade twisting to get optimum angle attack has great significance on blade design.
- Mixed airfoils are not usually used for a small-scale wind turbines. However, this work has shown that mixed airfoil wind turbine has satisfactory performance in small wind energy sector.
- The application of different correction models has viable effect on BEM analysis. The stall and wake correction model are also necessary options to improve accuracy of the BEM analysis.
- The detailed flow characterization by CFD has a great impact on performance prediction and optimization of wind turbine blade design. Comparing with the BEM method, CFD analysis can produce more accuracy in power prediction of wind turbine blade.

- To overcome the drawbacks of a horizontal axis wind turbine, Vortex bladeless wind turbine can be a reliable source for small scale wind energy sector.

5.1 Recommendations for Future Work

Though lots of research work has been done and continuously going on wind technology, there are still scopes to accelerate the revolution in this sector. Based on the research work done by this study, the further research works are recommended below.

- The integration of tower, rotor hub, generator housing, and yaw control have much effect on overall efficiency of the wind turbine. This research concentrated on only turbine blade design. The auxiliary parts can be added to research for a complete small scale wind turbine model analysis.
- The structural development of the currently designed wind turbine blade could be made by FSI analysis and several optimizing techniques.
- Different types of airfoil could be used at a time to design the blade, as well as pitch angles, could be varied to get better performance.
- In CFD Different meshing methods and different solving model could be used to explore better outcome.
- For vortex bladeless wind turbine, there are still huge scopes to investigate the potentiality of this new concept. A detailed analysis of Fluid Structure Interaction (FSI) could be a viable application to determine power and performance of the vortex bladeless wind generator.
- Another important challenge of vortex bladeless wind turbine is the orientation and integration of generator. The piezoelectric material or linear energy harvester could be a reliable solution for generators.

REFERENCES

A. j. Vitale, A. R. (2008). Computational method for the design of wind turbine blades. *International Journal of Hydrogen Energy*, 3466-3470.

ANSYS Inc. (2009). *Turbulence models ANSYS FLUENT 12.0 Theory Guide.* ANSYS Inc.

AWEA. (2016, March 3). *Wind Energy Facts at a Glance*. Retrieved from American Wind Energy Association : http://www.awea.org/wind-energy-facts-at-a-glance

Bearman, P. W. (1984). Vortex shedding from oscillating bluff bodies. *Annual review of fluid mechanics* , 195-222.

Breton.S.P., C. &. (2008). A study on rotational effects and different stall delay models using a prescribed wake vortex scheme and NREL phase VI experiment data. *Wind Energy*, 459-482.

Burton, T., Sharpe, D., Jenkins, N., & Bossany, E. (2001). *Wind Energy Handbook.* West Sussex: Jhon Wiley & Sons Ltd.

C. Bak, J. J. (2006). Three-dimensional corrections of aerofoil characteristics based on pressure distributions . *European Wind Energy Conference.*

Chen, X. (2014). Extreme value distribution and peak factor of crosswind response of flexible structures with nonlinear aeroelastic effect. *Journal of Structural Engineering*, 04014091.

Crawford, C. (2006). Re-examining the precepts of the blade element momentum theory for coning rotors. *Wind Energy*, 10.1002/we.197.

D. Hu, Z. D. (2006). A study on the static stall for horizontal axis wind turbine. *Taiyangneng Xuebao/Acta Energiae Solaris Sinica*, 217-222.

David Hartwanger, &. A. (2008). 3D modeling of a wind turbine using CFD. *NAFEMS Conference.* United Kingdom.

Davood Saeidi, A. S. (2013). Aerodynamic design and economical evaluation of site specific small vertical axis wind turbines. *Applied energy* , 101, 765-775.

Du.Z & Selig.M.A. (1998). A 3-D stall-delay model for horizontal axis wind turbine performance prediction. *ASME Wind Energy Symposium* (pp. AIAA-98-0021). Reno: American .

Duffy, M. J. (2010). *SMALL WIND TURBINES MOUNTED TO EXISTING STRUCTURES.* Georgia Institute of Technology .

E. Dimitriadis, D. M. (2014). Investigation of the performance of a horizontal axis wind turbine with the use of blade element momentum theory and CFD computations. *European Wind Energy Association*, (p. Barcelona).

E.C. Douvi, &. D. (2014). Computational study of the flow over a horizontal axis wind turbine. *6th International Conference from "Sci"*. Patras: IC-SCCE.

El-Shahat, A. (2016). Nanogrid Technology Increasing, Supplementing Microgrids. *Natural Gas Electricity*, V-33, N-2.

Enerdata. (2016, March 14). *Global Energy Statistical Yearbook*. Retrieved from Enerdata intelligence & consultancy website: https://yearbook.enerdata.net/renewable-in-electricity-production-share-by-region.html

Fluent, A. 1. (2009, March 1). *User's Guide, Fluent Inc.* New Hampshire: Ansys inc. Retrieved from Ansys User's Guid.

Gabbai, R. D. (2005). An overview of modeling and experiments of vortex-induced vibration of circular cylinders. *Journal of Sound and Vibration*, 282(3), 575-616.

Gaurao Gohate, S. B. (2016). Study of Vortex Induced Vibrations for Harvesting Energy. *International Journal for Innovative Research in Science & Technology*, 2349-6010.

Graebel, W. (2007). *Advanced fluid mechanics.* Academic Press.

Green, S. I. (1995). Fluid Vortices. *Fluid Mechanics and Its Applications*, vol. 30.

GWEC. (2017). *Global Wind Statistics 2016.* Brussels: Global Wind Energy Council.

Hansen, p. j. (2005). *AeroDyn theory manual.* Golden: National Renewable Energy Laboratory.

Harshith K, B. S. (2016). Bladeless Wind Power Generation. *International Journal for Scientific Research & Development*, 2321-0613.

Hills, R. L. (1994). *Power from Wind.* Cambridge: Cambridge University Press.

Hiroyuki Hirahara, M. Z. (2005). Testing basic performance of a very small wind turbine designed for multi-purposes. *Renewable energy*, 30.8,1279-1297.

Jacobs., M. L. (1961). *Experience with Jacobs wind-driven electric generating plant, .*

Jai N. Goundar, a. M. (2013). Design of a horizontal axis tidal current turbine. *Applied energy* , 161-174.

Jiménez, A. (2009). Analysis of a wind turbine wake using a LES method. Application to wake meandering. *Euromech Colloquim on wind turbine wakes.* Madrid.

Jmaes Tangler, D. K. (2004). Wind Turbine Post-Stall Airfoil Performance Characteristics Guidelines for Blade-Element Momentum Methods. *43rd AIAA Aerospace Science Meeting and Exhibit* (p. 591). Reno: Aerospace Research Central.

Joshua Yen, &. N. (2012). Improving safety and performance of small-scale vertical axis wind turbines. *Procedia Engineering*, 49, 99-106.

L. Wang, R. Q. (2016). Fluid-structure interaction modeling of horizon-tal-axis wind turbine blades based on CFD and FEA. *Journal of Wind Engineering and Indus-trial Aerodynamics*, 158,11-25.

L. Wang, X. T. (2012). Optimized chord and twist angle distributions of wind turbine blade considering Reynolds number effects. *Wind Energy: Materials, Engineering and Policies (WEMEP).*

Lissaman, P. B. (1983). Low-Reynolds-number airfoils. *Annual Review of Fluid Mechanics*, 15(1), 223-239.

Luisa C. Pagnini, B. M. (2015). Experimental power curve of small-size wind turbines in turbulent urban environment. *Applied Energy*, 154, 112-121.

M. K. Emam, G. E. (2015). A Comparative study between analytical and CFD analysis for performance prediction of a horizontal axis wind turbine. . *En-gineering Research Journal*, 145,M1-M14.

M. Keerthana, S. k.-s. (2012). Aerodynamic analysis of a small horizontal axis wind turbine using CFD. *Journal of Wind and Engineering*, 14-28.

M.A. Yurdusev, R. A. (2006). Assessment of optimum tip speed ratio in wind turbines using artificial neural network. *Energy*, V 31.12, 2153-2161.

Manwell, J., & McGowan, J. &. (2009). *Wind Energy Explained: Theory, Design & Application.* West Sussex: A Jhon Wiley & Sons Ltd.

Marshall, L. B. (2005). *A new empirical relationship between thrust coefficient and induction factor for the turbulentwindmill state.* Golden: National Renewable Energy Laboratory.

Mathew, D. S. (2006). *Wind Energy fundamentals resource analysis and economics.* Heidelberg: Springer.

Mathew, S. (2006). *Wind Energy Fundamentals, Resource Analysis and Economics.* Tavanur Malapuram: Springer-Verlag Berlin Heidelberg.

Mckenna, P. (2015). *Bladeless wind turbines may offer more form than function.* MIT Technology Review.

Miley, S. J. (1982). *A catalog of low Reynolds number airfoil data for wind turbine applications.* College Station: Rockwell International Corporation.

Mohammad Sriti, a. Y. (2016). Performance prediction of a horizontal axis wind turbine using BEM and CFD methods. *MATEC Web of Conferences* (p. Vol 45). EDP Sciences.

NREL. (2017, March 10). *NWTC Information Portal*. Retrieved from National Renewable Energy Labratory: http://wind.nrel.gov/airfoils/shapes/S833_Shape.html

P. Giguere, a. M. (1998). New airfoils for small horizontal axis wind turbines. *Journal of solar energy engineering* , 120.2 108-114.

Patel Hardik, a. D. (2013). Performance Prediction of Horizontal Axis Wind Turbine Blade. *Performance Prediction International Journal of Innovative Research in Science, Engineering and Technology*, Vol 2 Issue 5.

Peter Fuglsang, C. B. (2004). Design and Vericfiction of the Riso-B1 Airfoil Family for Wind Turbine. *Journal of Solar ENERGY ENGINEERING* , 1002-1010.

Putnam, P. C. (1948). *Power From the Wind.* New York: Van Nostrand Reinhold.

R. Lanzafame, M. M. (2007). Fluid dynamics wind turbine design : critical analysis,optimization and application of BEM theory. *Renewable Energy*, 2291-2305.

R. S. Amano, &. R. (2009). CFD analysis on aerodynamic design optimization of wind turbine rotor blades. *International Journal of Mechanical, Aerospace, Industrial, Mechatronic and Manufacturing Engineering*, 71-75.

Ragheb, M., & Adam, M. R. (2011). Wind Turbines Theory - The Betz Equation and Optimal Rotor Tip Speed Ratio . In D. R. Carriveau, *Fundamental and Advanced Topics in Wind Power*. Rijeka: Intech open science.

Ronit K Singh, a. M. (2013). Blade design and performance testing of a small wind turbine rotor for low wind speed applications. *Renewable Energy*, 812-819.

Rostami, A. B. (2017). Renewable energy harvesting by vortex-induced motions: Review and benchmarking of technologies. *Renewable and Sustainable Energy Reviews*, 193-214.

S. Eriksson, H. B. (2008). Evaluation of different turbine concepts for wind power. *Renewable and Sustainable Energy Reviews*, 12(5), 1419-1434.

Salih, B. (2014). An Introductory Study of the Dynamics of Autorotation for Wind Energy Harvesting. Florida, USA: University of Central Florida.

Simona Culotta, V. F. (2015). Small Wind Technology Diffusion in Suburban Areas of Sicily. *Sustainability*, 12693-12708.

Somers, D. M. (2005). *The S822 and S823 airfoils* . Golden: National Renewable Energy Laboratory, USA. NREL/SR-500-36342.

Somers, D. M. (2005). *The S833 S834 S835 Airfoils* . Pennysylvania: Port Matilda.

Tony Burton, D. S. (2004). *Wind energy handbook.* New York: John Wiley &Sons Ltd.

U.S. eia. (2016, March 14). *Electric Power Monthly*. Retrieved from U.S. Energy Information Administration Web site: https://www.eia.gov/electricity/monthly/

U.S. Energy Department, W. E. (2015, November 09). *Energy Efficiency & Renewable Energy*. Retrieved November 09, 2015, from http://apps2.eere.energy.gov/wind/windexchange/windmaps/

Viterna Larry A., a. J. (1982). Theoretical and experimental power from large horizontal-axis wind turbines. *Energy Production and Conversion.* Cleveland: Nasa.

Vowles, H. P. (1930). An inquiry into the origins of the windmill. *Journal of the Newcomen Society* , 11,1-4.

Vowles, H. P. (1932). Early evolution of power engineering. *A journal of the History of Science Society*, 412-420.

W.A. Timmer, R. P. (2003). Summary of the Delft University wind turbine dedicated airfoils. *Journal of Solar Energy Engineering* , 488-496.

Wilson, R. E. (1976). *Aerodynamic Performance of Wind Turbine.* Corvallis: Aerovironment inc.

Wu Jie-Zhi, H.-Y. M.-D. (2007). *Vorticity and vortex dynamics.* Springer Science & Business Media.

WWEA . (2015). *Small Wind World Report 2015.* Bonn: World Wind Energy Association.

Xinzi Tang, X. L.-k. (2009). Rotor design and analysis of stall-regulated horizontal axis wind turbine. *Universities Power Engineering Conference (UPEC), 2009 Proceedings of the 44th International. IEEE.*

Yukio Watanabe, H. I. (2007). Shape optimum design of horizontal axis wind turbine in low Reynolds number range. *European Wind Energy Conference.* Milan.